The Reference Frame for Encoding and Retention of Motion Depends on Stimulus Set-size

D. Huynh[1], S.P. Tripathy[4], H.E. Bedell[2,3], H. Öğmen[1,2,5*]

[1]Department of Electrical and Computer Engineering, University of Houston, Houston TX USA.

[2]Center for Neuro-Engineering and Cognitive Science, University of Houston, Houston TX USA.

[3]College of Optometry, University of Houston, Houston TX USA.

[4]School of Optometry and Vision Science, University of Bradford, U.K.

[5]Department of Electrical and Computer Engineering, University of Denver, Denver CO USA.

*Correspondence to: Haluk Öğmen, Department of Electrical and Computer Engineering, University of Denver, Denver CO 80208, USA. Phone: 303-871-2621. Fax: 303-871-2716. E-mail: ogmen@du.edu

ABSTRACT

The goal of this study was to investigate the reference frames used in perceptual encoding and storage of visual motion information. In our experiments, observers viewed multiple moving objects and reported the direction of motion of a randomly selected item. Using a vector-decomposition technique, we computed performance during smooth pursuit with respect to a spatiotopic (non-retinotopic) and to a retinotopic component and compared them with performance during fixation, which served as the baseline. For the stimulus encoding stage, which precedes memory, we found that the reference frame depends on the stimulus set-size. For a single moving target, the spatiotopic reference-frame had the most significant contribution with some additional contribution from the retinotopic reference-frame. When the number of items increased (set sizes 3 to 7), the spatiotopic reference-frame was able to account for the performance. Finally, when the number of items became larger than 7, the distinction between reference frames vanished. We interpret this finding as a switch to a more abstract non-metric encoding of motion direction. We found that the retinotopic reference frame was not used in memory. Taken together with other studies, our results suggest that, whereas a retinotopic reference frame may be employed for controlling eye-movements, perception and memory use primarily non-retinotopic reference-frames. Furthermore, the use of non-retinotopic reference frames appears to be capacity limited. In the case of complex stimuli, the visual system may use perceptual grouping in order to simplify the complexity of stimuli or resort to a non-metric abstract coding of motion information.

Key Words: Motion perception, reference frame, sensory memory, iconic memory, short-term memory.

INTRODUCTION

The optics of the eyes map the three-dimensional visual scene into two-dimensional retinal images. The projections from retina to sub-cortical and to early visual cortical areas preserve the neighborhood relationships in these images, creating what is known as *retinotopic representations* (Engel, 1994; Gardner et al., 2008; Sereno et al., 2001; Tootell et al., 1995, 1998). Retinotopic representations are informative about the position of stimuli in the scene with respect to the eyes and hence can play a role in the control of eye movements (McKenzie & Lisberger, 1986). For example, to make a saccade to a selected stimulus, sensorimotor systems can compute the "error signal", i.e., the distance of the target with respect to fovea, within retinotopic representations and use the error signal to program the movements of the eyes (McKenzie & Lisberger, 1986; Orban de Xivry & Lefèvre, 2007). There is also evidence that spatiotopic representations, i.e., representations based on reference frames that are located in space, contribute to the control of eye-movements (Mays & Sparks, 1980; Pertzov, Avidan, & Zohary, 2011). On the other hand, retinotopic representations are not well suited to explain our perceptual experience under normal viewing conditions due to the movements of the observer (eye, head, body movements, which we call "ego-motion") and those of the objects in the environment (which we call "exo-motion").

Natural human vision is based on a sequence of saccadic or smooth gaze changes that direct the fovea to and maintain it on stimuli of interest (Buswell, 1935; Yarbus, 1967; Zelinsky & Todor, 2010). These ego-motions cause drastic shifts of stimuli in retinotopic representations. Despite this instability in retinotopic representations, our perceptual experience of the visual world appears to be highly stable. It stands to reason that other coordinate systems, that we will call collectively as *non-retinotopic representations*, are necessarily involved for the visual system to achieve a sense of spatiotemporal coherence (Bridgeman et al., 1994; Melcher & Colby, 2008; Wurtz, 2008; Cavanagh et al., 2010; Burr & Morrone, 2011, 2012; Melcher & Morrone, 2015). It has been suggested that efference-copy signals associated with ego-motion commands play an important role in transforming retinotopic representations into non-retinotopic representations (Von Helmholtz, 1925; Von Holst, 1954; Mack, 1986; Andersen et al., 1993; Bridgeman, 1995). In addition to stabilizing our percepts, the inclusion of efference-copy signals to build up non-retinotopic representations may also improve abilities such as localization of speed differences in complex stimuli. For example, Braun et al. (2010) measured thresholds for detecting the spatial location of stimuli that undergo speed changes

during fixation and smooth pursuit. They showed that the ability to spatially localize speed changes was better during pursuit compared to fixation, which they attributed to the use of efference-copy signals (Braun et al., 2010).

Another problem for retinotopic representations stems from the movements of objects in the environment (Burr, 1980; Chen et. al., 1995; Nishida, 2004; Öğmen, 2007; Öğmen & Herzog, 2010). When objects in the environment move (exo-motion), they activate retinotopically anchored mechanisms only briefly and hence the resulting percepts are predicted to be blurred with "ghost-like" appearances (Öğmen, 2007; Öğmen & Herzog, 2010). However, our percepts of moving objects are in general sharp and clear. In the case of exo-motion, it has been suggested that the motion of objects are used to build reference frames to transform retinotopic representations into non-retinotopic representations (Duncker, 1938; Wade & Swanton, 1987, 1996; Bremner et al., 2005; Noory, Herzog, & Öğmen, Herzog, 2015).

In addition to the question of which reference frames are used to explain our motor behavior and our real-time perceptual experience, it is also important to understand the reference frames used in memory systems. According to the modal model of human memory (Atkinson & Shiffrin, 1968; Baddeley & Hitch, 1974), the visual stimulus-encoding stage is followed by three memory systems: Visual-Sensory memory (VSM), Visual-Short-Term Memory (VSTM), and Long-Term Memory (LTM).

Whereas much of the research on VSM indicates that it is encoded in retinotopic coordinates (e.g. Haber, 1983; Jonides et al., 1983; Rayner & Pollatsek, 1983; Irwin et al., 1983, 1988; Sun & Irwin, 1987), more recent findings using sequential metacontrast and Ternus-Pikler displays indicate that sensory memory can also employ motion-based non-retinotopic reference frames (Öğmen, 2007; Öğmen & Herzog, 2010; Noory, Herzog, & Öğmen, 2015).

Studies on the reference frames underlying VSTM have been equivocal. In a study by Baker et al. (2003), monkeys were trained to hold in memory either the retinotopic or spatiotopic location of a stimulus, and then, after a slow gaze shift (smooth pursuit eye movement), make a saccade towards the remembered location. They found that saccades to spatiotopic locations are more variable than saccades to retinotopic locations, and suggested a retinotopically organized model of VSTM for spatial information. Retinotopic processing in VSTM was also suggested by Golomb and Kanwisher (2012) based on the finding that, after making a visually guided saccade during a memory-delay interval, observers were significantly more accurate and precise at reporting retinotopic locations

than spatiotopic locations. Results from study by Ong et al. (2009), on the contrary, favor the spatiotopic model of VSTM. In a delayed-saccade paradigm, observers were asked to compare directions of motion of a pre-saccadic and a post-saccadic stimulus. Performance was found optimal when the two stimuli appear at the same spatiotopic, rather than retinotopic, location.

Given the important role that motion information carries in visual processing and given that motion itself can constitute a reference frame, the goal of our study was to investigate the reference frames used in the encoding and the retention of motion information in VSM and VSTM. In principle, to distinguish retinotopic and non-retinotopic components of visual processing, one has to manipulate movements of the observer (e.g., the eyes) and of the objects, because the two systems are not separable under static viewing. Most of the previous work investigating reference frames for visual memory reviewed earlier was based on procedures that involved saccadic eye movements. The use of only vertical and/or horizontal saccadic displacements of the eyes and highly predictable locations of objects might limit the generality of those findings. In addition, although visual stimuli were defined on the basis of attributes such as orientation or motion, their spatial location was the only factor used to contrast retinotopic and non-retinotopic conditions. In the present study, with eye displacements incorporated in the form of smooth-pursuit eye movements (SPEMs), we dissociated the two reference frames by applying motion-vector decomposition (see Data Analysis Section). Directions of eye and object movements were both randomized in our experiments. We sought to investigate the coordinates in which the visual system encodes and stores in memory the directions of motion of multiple moving stimuli.

Previous studies addressing reference frames for motion stimuli mostly focused on processing at the perceptual encoding level. The perceived direction of motion during pursuit has been reported to have retinotopic (Becklen et al., 1984; Festinger et al., 1976; Mateeff, 1980; Wallach et al., 1985) and incompletely converted spatiotopic coordinates (Souman et al., 2005a; Souman et al., 2005b; Souman et al., 2006a; Souman et al., 2006b; Swanston & Wade, 1988). In terms of attentively tracking the identities of multiple moving-objects, it has been suggested that both retinotopic and spatiotopic coordinate systems are used (Howe, Pinto, Horowitz, 2010). A more recent study showed that the effective reference frame for motion consists of an integration of motion-based, retinotopic and spatiotopic reference frames (Agaoglu et al., 2015a, 2015b). However, very few studies have investigated reference frames underlying memory for motion. Melcher and Fracasso (2012) investigated the trans-saccadic line-motion illusion (TLMI) by introducing a saccade between the

presentation of the inducer and the line. They also presented two inducers on each trial such that any illusion operating in a retinotopic reference frame would be in opposition to any illusion in a spatiotopic reference frame. The study found that the direction of the TLMI perceived was largely consistent with a spatiotopic reference frame. In a separate experiment the authors varied the number of inducers in the TLMI stimulus and found that observers had a capacity of approximately two inducers, well below the capacity of about seven that they found in a comparable trans-saccadic visual working memory experiment for color. They suggested the trans-saccadic capacity was limited by the number of object files or attentional pointers that could be updated across saccades. It is not clear how this TLMI study would generalize to other motion tasks, because in TLMI the inducers used in the memory task were stationary, as was the line, and the percept in line motion illusion differs from that in apparent motion, though there is some overlap of the neural mechanisms involved in the two tasks (e.g. Jancke, Chavane, Naaman & Grinwald, 2004).

In this study, using a partial-report technique, in which the cue was delivered immediately, or else with varying delays, after stimulus offset, we examined perception of motion in the different processing stages, from encoding to sensory memory and VSTM. We determined reference systems for each stage of motion processing in two conditions, with and without eye movements. With eye movements (SPEM condition), non-retinotopic and retinotopic coordinates are dissociable. In general, if motion is processed primarily in one coordinate system, performance measured in that system during SPEM should be better than that measured in the other system. Also, the former should be comparable to the performance level in the absence of eye movements (fixation condition, in which case, non-retinotopic performance is the same as retinotopic performance).

Previous studies have varied set-size in order to get estimates of capacity of the visual system for processing multiple motions in a variety of tasks involving: tracking of object identities (Pylyshyn & Storm, 1988); monitoring changes in direction of motion (Tripathy & Barrett, 2004; Tripathy, Narasimhan & Barrett, 2007; Narasimhan, Tripathy & Barrett, 2009); monitoring directions of motion (Horowitz & Cohen, 2010; Shooner, Tripathy, Bedell & Öğmen, 2010); encoding and memory of directions of motion (Öğmen, Ekiz, Huynh, Tripathy & Bedell, 2013); and feature-binding (Huynh, Tripathy, Bedell & Öğmen, 2015). An open question is whether a single reference frame is used for processing motion across all set-sizes. Several recent studies point to the existence of multiple complementary mechanisms for processing multiple objects, in particular, low-capacity systems that can process 3-4 items individually, and high-capacity systems for encoding and storing

summary statistics of sets/groups/ensembles of objects larger than the aforementioned 3-4 items (Cant, Sun & Xu, 2015). The summary statistics that are extracted during ensemble coding include means or averages (reviewed in Bauer, 2015) and variances (Norman, Heywood & Kentridge, 2015). Ensemble coding has been demonstrated for a variety of features including low-level ones such as mean size (Ariely, 2001; Corbett & Melcher, 2014), variance in orientation (Norman, Heywood & Kentridge, 2015), and high-level features such as averages of emotions, gender and identities of faces, and behaviors of crowds (Haberman & Whitney, 2007; de Fockert & Wolfenstein, 2009; Sweeny, et al., 2012). It is likely that different mechanisms are involved in the extraction of summary statistics of different features (Hubert-Wallander & Boynton, 2015), making generalizations difficult. Studies of ensemble encoding usually require observers to report some average statistic of some stimulus feature, rather than some feature pertaining to one particular object as in our partial report experiments. However, some contribution of ensemble encoding to the measured capacity cannot be ruled out (Brady & Alvarez, 2015). We varied set-size between 1 and 12 in order to estimate the capacity of the motion system for representing direction of motion at the encoding and memory stages. The range of set-sizes permits us to investigate if different mechanisms operate at small and large set-sizes, using potentially different reference frames.

Statistical modeling further allowed us to determine whether a purely non-retinotopic, retinotopic, or a combined model best describes the behavioral data, as well as to probe the quantitative and qualitative details of observers' performance.

METHODS

We ran a set of four experiments in which observers tracked multiple moving objects while: (1) maintaining their gaze on a fixation point (Experiments 1a-1b); or (2) performing a Smooth Pursuit Eye Movement - SPEM (Experiments 2a-2b). The task of the observers was to report the perceived direction of motion of a randomly chosen object by rotating an on-screen pointer. Experiments 1a and 2a, in which the target to be reported was cued immediately after objects stopped moving and disappeared, aimed to characterize the initial encoding stage. While observers had to hold in memory information about this cued target during the reporting phase, having a single target item and no delay after stimulus offset minimized the involvement of memorization in their performance.

Experiments 1b and 2b included varying cue delays, aimed to tap into sensory memory and VSTM. For each eye movement condition, we provided observers with several initial training blocks (28 trials each) to ensure that each of them could perform all tasks well. In general, a reasonable proportion of valid trials (> 70%) was obtained after 2 or 3 such blocks. Criteria for the validity of a trial in the fixation and SPEM conditions are described below under the procedure of experiments 1a and 2a, respectively. These criteria were applied for only the dominant eye of each observer, which was determined in advance using the ABC test for sighting dominance (Miles, 1929, 1930). We used the dominant eye because subjects fixate significantly more accurately with the dominant eye compared to the non-dominant eye during eye-position calibration (Nyström et al., 2013; Vikesdal & Langaag, 2016) and track more faithfully target motion with the dominant eye (Gibaldi et al., 2016). One participant had a left dominant eye (TTN), the remaining three had right dominant eyes (TAN, QVP, DHL). Eye positions for both eyes were recorded, but only the dominant eye's data were used in analyses. In addition, a short training block (7 or 14 trials) was also run when observers came back after a break to foster stability of performance.

Participants: The first author and 3 naïve observers with normal, or corrected to normal visual acuity, and with no color deficiency (according to self-reports and the online version of the Ishihara test) participated in all experiments. Naïve observers were not informed about the hypotheses of the study. Experiments were conducted according to a protocol adhering to the Declaration of Helsinki and approved by the University of Houston Committee for the Protection of Human Subjects.

Apparatus: A Visual Stimulus Generator system (Cambridge Research Systems) with a VSG2/5 video card housed in a personal computer and a SONY GDM-FW900 color monitor (20 inches, 100 Hz) were used to create and display stimuli; programming was implemented in C++. The screen resolution was 800x500 pixels of which 604x405 pixels (19.7x13.2 deg; 1.96 arcmin/pixel) were used for object display. The screen edges were visible during the experiments, but the border of the display area was not. Observers used a computer mouse to give their response, and their heads were kept still on a head/chin rest at a distance of 1 meter in front of the monitor. Gaze position and velocity were recorded using a head-mounted binocular eye tracking system (SR Research – Eyelink II) sampling at 250 Hz.

Stimuli: A black cross subtending 1.5x1.5 deg was used to guide eye fixation or pursuit movements. Objects were circular disks of different readily distinguishable colors that were randomly selected from a set of 180 equi-luminant colors. These 180 colors were sampled along a circle (i.e., resolution

2°/color) in the CIE L*a*b color system. The circle is located at L = 15 cd/m^2, centered at the white point (with a = 0.2044 and b = 0.4808), and its radius was chosen to maximize the discriminability of the colors (approximately 2°). Color separation of any two objects was not smaller than 17° (see Huynh et al., 2015 for a justification of this separation). Although color was task-irrelevant in the present experiments, we used colored instead of uniform gray objects, as in the Huynh et al. study, for comparison purposes. The diameter of each object was chosen to subtend a visual angle of 1 deg. Objects were presented on a gray 40-cd/m^2 background.

Experiment 1a: ***Reference Frames for Stimulus Encoding during Fixation***

Procedure: A trial began with a fixation-cross presented at the center of the screen. Observers were instructed to start fixating the cross when ready and promptly click the mouse. Upon detecting this mouse click, the program sent a trigger code to the eye tracker. An on-line drift correction was performed and eye movement recordings started at this point. Observers continued to hold fixation on the cross. At 1300 ms after the mouse click[1], a stimulus containing multiple moving disks was displayed for 200 ms while the fixation cross remained stationary. The disks moved along linear trajectories in random directions at a speed of 5 deg/s. To minimize interference between the objects, the disk trajectories were constrained never to cross one another and no two objects had motion directions closer than 17 deg. After 200 ms of presentation, the stimuli were removed from the display. One of the disks was randomly chosen to be the probed item, the position of which was cued by a small black dot, and observers were asked to report the disk's motion direction by rotating an on-screen pointer, which was a black bar extending from the dot, to the perceived direction (Figure 1). Although the fixation cross remained visible until response, eye tracking ended and fixation was no longer strictly required after the offset of the stimuli.

----- insert Figure 1 here -----

Note that the present experiments were different than our previous experiments in Huynh et al. (2015) in that: (1) No static preview of objects (1 s) was shown before the motion period as we wanted the objects to only appear during the steady phase of smooth pursuit; and (2) No feedback was provided after responses in either the training or experimental runs. Because gaze position was

[1] The choice of this duration was to make it consistent with the SPEM condition to be described later.

controlled in the present experiments, observers might learn from feedback and adjust their responses to avoid errors that they realized they made repeatedly when the target moved across their gaze point at certain distances or directions.

As mentioned earlier, gaze position was monitored by the eye tracker. During each trial, observers were asked to maintain their gaze on the fixation point at the center of the screen until the disk stimuli disappeared. To be considered as a good fixation, observers' gaze had to remain within a circular area with 1-deg radius around the central point of the cross, with no saccades or blinks. If any of these requirements were not met, the trial was rejected and observers received text feedback on the display telling the reason for rejection. The rejected trial was repeated later during the same set of trials.

Design: Seven set sizes (one, three, four, six, eight, nine, or twelve) of moving objects were tested. The experiment was divided into 25 separate blocks with trials of all set sizes randomly interleaved within each block. A block ended whenever observers finished 28 valid trials (4 trials per condition of set size). That is, each observer ran 4*25 = 100 trials per set size, or 700 trials in total. The eye tracker was recalibrated at the start of each block using a 9-point grid. Calibration validation was checked twice, after the calibration and when the observer completed a block. If any of the fixated positions during validation disagreed from the original calibration by more than 1.5 deg at the conclusion of any block, the entire block was excluded and re-run later.

Experiment 1b: ***Reference Frames for Sensory Memory and VSTM during Fixation***

Experiment 1b was the same as experiment 1a except for the following changes:

- The number of objects was fixed at 6 in every block.
- The cue was not always given immediately after the objects disappeared but was preceded by a variable-duration delay. Seven different delay values (0, 50, 100, 250, 500, 1000, or 3000 ms) were randomly chosen on each trial.

As in Experiment 1a, observers finished a block after obtaining 28 valid trials (4 trials per condition of cue delay). A total of 25 blocks yielded 4*25=100 trials per condition of cue delay, or 700 trials in total. Observers followed the same steps as in Experiment 1a. Invalid trials and blocks were discarded and re-run.

Experiment 2a: ***Reference Frames for Stimulus Encoding during SPEM***

Procedure: We applied the step-ramp paradigm devised by Rashbass (1961) to obtain a relatively fast and smooth initiation of pursuit eye movement (Figure 2). A cross of the same design as in the fixation condition served as the pursuit target. Observers were required to fixate initially and then smoothly follow this target as it moved. At the beginning of each trial, the cross was presented at a randomly selected location on an invisible circle that was centered at the center of the screen and had a radius of 3 deg (in terms of visual angle). Observers were instructed to start fixating the cross when ready and promptly click the mouse. A command was then sent by the program to request the eye tracker to perform drift correction and start recording eye data. The cross remained stationary for 500 ms after the mouse click, then suddenly jumped in the centrifugal direction to another location which was at 4 deg away from the center of the screen (step size = 1 deg), and immediately started moving in the opposite direction toward the center at a constant speed (5 deg/s). The target reached the center of the display at 800 ms after the step and continued to move in the same direction for an additional 200 ms. The stimuli containing multiple moving disks were displayed during this 200 ms period (Figure 3). Similar to the fixation condition, the disks moved along linear trajectories in random directions at the speed of 5 deg/s, the same as that of the pursuit target. When the pursuit target stopped moving at 1 deg from the center point, the stimuli were removed from the display. A randomly chosen disk was marked immediately with a small black dot to indicate the target for response. The task of reporting the target's direction of motion was the same as in Experiments 1a and 1b.

----- insert Figure 2 here -----

Criteria for a valid smooth-pursuit trial

To guarantee that observers successfully performed smooth-pursuit eye movements while tracking the moving disks, a number of requirements had to be met. First, during the initial fixation phase, observers had to maintain their gaze within an invisible circle (1.5 deg radius) around the center of the cross. Second, given the pursuit latency on the order of 120 ms, pursuit onset had to be detected in the interval 120 – 600 ms after the step (Figure 2). Eye velocity ($\overrightarrow{v_e}$) had to exceed 25% of target velocity ($\overrightarrow{v_t}$) to be considered as pursuit onset. Third, we considered pursuit quality during the last 300 ms of pursuit, including the 200 ms of stimulus presentation and the previous 100 ms (Figure 2). An EyeLink II built-in function was employed to calculate average eye velocity. This

function allowed for the selection of the width of a moving window containing a certain group of most recent gaze-position samples that would be considered to estimate the velocity of the middle sample in the group, hence minimizing noise. In our pursuit experiments, we used the FIVE_SAMPLE_MODEL (width = 5 samples); with 4 ms/sample (EyeLink sample rate = 250 Hz). Therefore, 5 samples corresponded to 20 ms. By calling the function after each new sample, we obtained a running record of velocity for all samples during the last 300 ms of pursuit. Mean eye velocity over this interval was then computed separately for the horizontal ($|\overrightarrow{v_{ex}}|$) and vertical ($\left|\overrightarrow{v_{ey}}\right|$) components. To qualify as a smooth pursuit, pursuit gain ($PG = |\overrightarrow{v_e}|/|\overrightarrow{v_t}|$) and that for either of the two components ($PGx = |\overrightarrow{v_{ex}}|/|\overrightarrow{v_{tx}}|$ or $PGy = \left|\overrightarrow{v_{ey}}\right|/\left|\overrightarrow{v_{ty}}\right|$) had to fall in the range [0.7, 1.3]. We did not put this constraint on both PGx and PGy due to the fact that, when the direction of $\overrightarrow{v_t}$ was close to vertical or horizontal (rather small values of $|\overrightarrow{v_{tx}}|$ or $\left|\overrightarrow{v_{ty}}\right|$), it was virtually impossible to have the smaller component (PGx or PGy) fall in the specified range. Finally, also during the last 300 ms of pursuit, no saccades (saccade displacement threshold = 0.5 deg; saccade velocity threshold = 30 deg/s) or blinks were accepted. If any of the four constraints were violated, the trial was discarded and re-run during the same set of trials.

----- insert Figure 3 here -----

Design: Except for the difference in eye movement (smooth pursuit instead of fixation) and the corresponding criteria considered, the design of this experiment was the same as in Experiment 1a, with 7 set sizes and 100 valid trials per condition of set size. Observers also received text feedback about eye movement after each rejected trial, which was rerun in the same block of trials. Similar to experiments 1a and 1b, if post-block position calibrations disagreed with initial calibration values by more than 1.5 deg, the entire block was excluded and re-run later.

Experiment 2b: ***Reference Frames for Sensory Memory and VSTM during SPEM***

Experiment 2b was the same as experiment 2a except for the following changes:

- The number of objects was fixed at 6 in every block.
- The cue was not given always immediately after the objects disappeared but was preceded by a variable-duration delay. Similar to Experiment 1b, seven different delay values (0, 50, 100, 250, 500, 1000, or 3000 ms) were randomly chosen on each trial.

Again, observers ran 25 blocks to obtain 100 valid trials per condition of cue delay.

DATA ANALYSIS

Our goal was to use statistical models to break the observers' aggregate performance down into multiple components that characterize important aspects of their behaviors. This includes consideration of the extent to which correct target reporting, guessing and non-target misreporting account for variability of response errors, and the nature of the reference frames associated with these errors. We wished to obtain both qualitative and quantitative measures for each of these components. We analyzed and compared several plausible models that are different from one another in their assumptions about an observer's behavioral pattern. Our interpretations of the data were then based on the best performing model.

We used two different methods of fitting the models to empirical data (Huynh et al., 2015): *(1)* The method of Least Squares fitting involves the creation of a nonlinear optimization routine using the Matlab *fminsearch(.)* function to find the values of the parameters that minimize an error function; *(2)* The Expectation-Maximization (E-M) algorithm (Dempster et al., 1977), which employs Bayes' theorem for finding maximum likelihood estimates of the parameters. We found the best performing model by comparing adjusted R^2 (first method) and Akaike/Bayesian Information Criterion (second method) values obtained for each model and observed similar results. We report only the results of the first method in the main text. Mathematical derivation and results of the second method are provided in Supplemental Information.

The first four of our hypothetical models (models F1, F2, F3c, F3r) are the same as in our previous study (Huynh et al., 2015). These models take into account noise and uncertainties in an observer's responses and are independent of reference frames. They were used to analyze the fixation condition because stimulus motion is the same according to retinotopic and non-retinotopic coordinates in this condition. In the smooth pursuit condition, reference frame is incorporated into the models above as an additional factor. As shown in Figure 4, the motion of the stimulus is analyzed in terms of a non-retinotopic and a retinotopic reference frame. The non-retinotopic reference frame refers to the motion of the stimulus on the monitor display and we refer to this as the *spatiotopic coordinates*. By taking into account the eye movement velocity, the motion of the stimulus can also be represented as a retinotopic motion-vector, which is referred to as *retinotopic*

coordinates. We considered three different scenarios: (a) motion is processed only in spatiotopic coordinates (models SP1_S, SP2_S, SP3c_S, SP3r_S), (b) motion is processed only in retinotopic coordinates (models SP1_R, SP2_R, SP3c_R, SP3r_R), and (c) both spatiotopic and retinotopic coordinates are used, or perhaps there is a gradual transition from one to the other such that they become active simultaneously (models SP1_SR, SP2_SR, SP3c_SR, SP3r_SR).

----- insert Figure 4 here -----

We present below the models used in our analyses; the detailed explanations of these models are provided in the Supplemental Information section. Briefly, the error distribution obtained from the data is fitted by an embedded family of statistical distributions. The member of the family that provides the "best fit" is selected to interpret the data. As explained below, parameters of the model are interpreted in terms of observer's accuracy, precision, guess rate, and misbinding errors.

Fixation-Condition Models

Model F1: *Gaussian*

This model is the cumulative distribution function of a circular (wrapped) Gaussian:

$$\mathrm{CDF}(\varepsilon) = \mathrm{CDF}\{\mathrm{G}(\varepsilon; \mu, \sigma)\}, \quad (1)$$

where the cumulative distribution function $\mathrm{CDF}(\varepsilon)$ of the error variable ε (ε = reported direction of motion - actual direction of motion) is given by a Gaussian distribution $\mathrm{G}(\varepsilon; \mu, \sigma)$ whose parameters represent the accuracy (mean: μ) and the precision ($1/\sigma$, where σ is the standard deviation) of processing. The precision parameter $1/\sigma$ captures the qualitative aspect of performance, with smaller values of σ corresponding to higher qualities of encoding for the processed items.

Model F2: *Gaussian + Uniform*

In this model (Zhang & Luck, 2008), the distribution of errors is represented by:

$$\mathrm{CDF}(\varepsilon) = \mathrm{CDF}\{w.\mathrm{G}(\varepsilon; \mu, \sigma) + (1 - w).\mathrm{U}(-180,180)\}, \quad (2)$$

where the cumulative distribution function $\mathrm{CDF}(\varepsilon)$ is obtained from the corresponding probability density function that consists of two components:

(a) A Gaussian distribution $\mathrm{G}(\varepsilon; \mu, \sigma)$ described in the Gaussian model

(b) A uniform distribution U over the interval (-180, 180), which represents guessing

The weight of the uniform distribution (1 - *w*) represents the proportion of trials in which observers base their responses on guesses rather than on the target information available. The weight *w* of the Gaussian captures the quantitative aspect of performance by providing a relative measure for the *intake* of encoding, with a larger value corresponding to a greater possibility that a response is based on having some access to information from the cued target. Traditionally, the term *capacity* is used in the literature, as opposed to *intake.* By definition, capacity refers to the *maximum* amount of information that can be processed and/or stored. Hence, capacity refers in general to a *fixed* property of the system. Implicit in the definition of capacity is the idea that performance is unaffected by set-size when it is smaller than the capacity. This condition does not hold for the perception of motion-direction, or changes in the direction of motion, where substantial drop in precision for reporting direction of motion (or increase in threshold when detecting deviations) is seen with increases of set-size, even for set-sizes of one or two (Tripathy & Barrett, 2004; Levi & Tripathy, 2006; Tripathy, Narasimhan & Barrett, 2007; Tripathy & Levi, 2008; Narasimhan, Tripathy & Barrett, 2009; Shooner et al, 2010; Öğmen *et al*, 2013; Huynh *et al*, 2015). This drop in performance with set-size necessitates an alternative way of characterizing the amount of information processed and/or stored in a given condition. For this purpose, we use the term *intake*, which represents the quantity of information processed/stored under a given stimulus condition (e.g., set-size). As an analogy, the capacity of a room can be 50 people (i.e., the maximum number of people in the room), whereas under a given situation the room may be holding only 26 people (intake). As mentioned above, research indicates that performance decreases with set-size in a continuous manner and a single capacity parameter is not adequate to characterize the amount of information that is processed and/or stored. Instead, using two parameters, one representing the variable *quantity* of information (intake) and a second one representing the *quality* of information (precision), appears to be a better theoretical approach (see for example the "leaky flask" model in Öğmen *et al*, 2013).

Models F3c and F3r: *Gaussian + Uniform + Gaussian*

These models (Bays et al., 2009) include an additional term to account for misbinding errors when observers get confused and report another object instead of the selected target:

$$\mathrm{CDF}(\varepsilon) = \mathrm{CDF}\left\{w.\,\mathrm{G}(\varepsilon;\mu_t,\sigma_t) + (1-w-w_m).\,\mathrm{U}(-180,180) + w_m.\,\mathrm{S}_{\mathrm{i}=1;\mathrm{i}\neq\mathrm{t}}^{\mathrm{T}}\left[\mathrm{G}\left(\varepsilon;\mu_t+\varepsilon_{i,t},\sigma_t\right)\right]\right\}, \quad (3)$$

where the first two terms represent the same Gaussian and Uniform distributions as in the Gaussian+Uniform model and the third term represents errors stemming from misbinding reports. The selection operator $S_{i=1;i\neq t}^{T}[.]$ determines which item from the set of (*T-1*) non-cued objects is the one that generates the subject's response due to a misbinding error. We analyzed two versions of this model— i.e., misbinding with the object that is closest to the cued target in either the cued-feature space (*closest cued-feature*: Position – model F3c) or the reported-feature space (*closest reported-feature*: Motion direction – model F3r).

Smooth-Pursuit Condition Models

For all models in this section, the error variable is denoted by ε_s to emphasize the fact that we consistently computed errors in spatiotopic coordinates. On the circular ring that represents all possible values of motion direction, the actual motion direction of the target coincides with the origin of the spatiotopic coordinate system. A conversion parameter is included where necessary to convert spatiotopic errors to equivalent retinotopic errors. The equations are similar if one prefers to compute errors in retinotopic coordinates, but the sign of the conversion parameter needs to be reversed.

Model SP1_S: *Spatiotopic Gaussian*

This model has the same form as model F1:

$$\mathrm{CDF}(\varepsilon_s) = \mathrm{CDF}\{\mathrm{G}(\varepsilon_s; \mu_s, \sigma_s)\}, \tag{4}$$

where μ_s and $1/\sigma_s$ respectively represent the accuracy and precision of spatiotopic processing.

Model SP1_R: *Retinotopic Gaussian*

This model also consists of the CDF of a circular Gaussian:

$$\mathrm{CDF}(\varepsilon_s) = \mathrm{CDF}\{\mathrm{G}(\varepsilon_s; \mu_r + \beta, \sigma_r)\}, \tag{5}$$

where μ_r and $1/\sigma_r$ respectively represent the accuracy and precision of retinotopic processing. The model assumes statistical analysis of retinotopic errors to produce a probability density function peaking near the actual retinotopic direction of motion and decaying for larger magnitudes of error. However, since the error variable ε_s is calculated with respect to the actual spatiotopic direction of motion, the mean of the Gaussian must be shifted from the origin by an angle β determined by the difference between the actual spatiotopic and retinotopic directions. This angle is given by (see Figure 4):

$$\beta = \sin^{-1}[\frac{|\overrightarrow{v_p}|}{|\overrightarrow{v_r}|}\sin\alpha]\,, \tag{6}$$

where $|\overrightarrow{v_p}|$ and $|\overrightarrow{v_r}|$ are the magnitudes of the pursuit and retinotopic motion vectors, respectively, and α is the angle between spatiotopic and pursuit motion vectors.

Model SP1_SR: *Spatiotopic Gaussian + Retinotopic Gaussian*

This model is the CDF of a weighted sum of two circular Gaussians:

$$\mathrm{CDF}(\varepsilon_s) = \mathrm{CDF}\{w_s.\,\mathrm{G}(\varepsilon_s;\mu_s,\sigma_s) + (1-w_s).\,\mathrm{G}(\varepsilon_s;\mu_r+\beta,\sigma_r)\}, \tag{7}$$

where the weights w_s and (1-w_s) represent the relative contributions (or *intakes*) of spatiotopic processing (with accuracy μ_s and precision $1/\sigma_s$) and retinotopic processing (with accuracy μ_r and precision $1/\sigma_r$), respectively. The means of the two components are separated by an angle β determined by equation (6).

Model SP2_S: *Spatiotopic Gaussian + Uniform*

This model has the same form as model F2:

$$\mathrm{CDF}(\varepsilon_s) = \mathrm{CDF}\{w_s.\,\mathrm{G}(\varepsilon_s;\mu_s,\sigma_s) + (1-w_s).\,\mathrm{U}(-180{,}180)\}\,, \tag{8}$$

where the first component is the Gaussian distribution described in model SP1_S, and the second component is a uniform distribution U over the interval (-180, 180), which represents guessing. The weights w_s and (1-w_s) represent the *intake* of spatiotopic processing and guess rate, respectively.

Model SP2_R: *Retinotopic Gaussian + Uniform*

This model also has two components:

$$\mathrm{CDF}(\varepsilon_s) = \mathrm{CDF}\{w_r.\,\mathrm{G}(\varepsilon_s;\mu_r+\beta,\sigma_r) + (1-w_r).\,\mathrm{U}(-180{,}180)\}\,, \tag{9}$$

where the first component is the Gaussian distribution described in model SP1_R, and the second component is a uniform distribution U over the interval (-180, 180), which represents guessing. The weights w_r and (1-w_r) represent the *intake* of retinotopic processing and guess rate, respectively. The angle β is determined by equation (6).

Model SP2_SR: *Spatiotopic Gaussian + Retinotopic Gaussian + Uniform*

This model combines models SP2_S and SP2_R and is represented by:

$$\mathrm{CDF}(\varepsilon_s) = \mathrm{CDF}\{w_s.\,\mathrm{G}(\varepsilon_s;\mu_s,\sigma_s) + w_r.\,\mathrm{G}(\varepsilon_s;\mu_r+\beta,\sigma_r) + (1-w_s-w_r).\,\mathrm{U}(-180{,}180)\}, \quad (10)$$

where the weights w_s, w_r and $(1-w_s-w_r)$ represent the relative contributions (or *intakes*) of spatiotopic processing (with accuracy μ_s and precision $1/\sigma_s$), retinotopic processing (with accuracy μ_r and precision $1/\sigma_r$), and guess rate, respectively. The means of the two Gaussian distributions are separated by an angle β determined by equation (6).

Models SP3c_S and SP3r_S: *Spatiotopic Gaussian + Uniform + Spatiotopic Misbinding Gaussian*

These models are similar to models F3c and F3r but all components are assumed to be only spatiotopic:

$$\mathrm{CDF}(\varepsilon_s) = \mathrm{CDF}\{w_s.\,\mathrm{G}(\varepsilon_s;\mu_s,\sigma_s) + (1-w_s-w_{sm}).\,\mathrm{U}(-180{,}180) + w_{sm}.\,\mathrm{S}^{\mathrm{T}}_{\mathrm{i}=1;\mathrm{i}\neq\mathrm{t}}\left[\mathrm{G}\left(\varepsilon_s;\mu_s+\varepsilon_{i,t},\sigma_s\right)\right]\}, \quad (11)$$

where the first two terms represent the same Gaussian and Uniform distributions as in model SP2_S and the third term represents errors stemming from misbinding. The weights w_s, w_{sm} and $(1-w_s-w_{sm})$ represent the *intake* of spatiotopic processing (with accuracy μ_s and precision $1/\sigma_s$), misbinding rate, and guess rate, respectively. The misbinding term is expected to also have a Gaussian distribution, with the same standard deviation as the first Gaussian but with the mean shifted from the first Gaussian by the difference $\varepsilon_{i,t}$ between the cued target's and the misbinding object's directions of motion. Similar to models F3c and F3r, models SP3c_S (*closest cued feature*) and SP3r_S (*closest reported feature*) differ in how the selection operator $S^{T}_{i=1;i\neq t}[.]$ determines the misbinding item from the set of (*T-1*) non-cued objects.

Models SP3c_R and SP3r_R: *Retinotopic Gaussian + Uniform + Retinotopic Misbinding Gaussian*

These models are similar to models F3c and F3r but all components are assumed to be only retinotopic:

$$\mathrm{CDF}(\varepsilon_s) = \mathrm{CDF}\{w_r.\,\mathrm{G}(\varepsilon_s;\mu_r+\beta,\sigma_r) + (1-w_r-w_{rm}).\,\mathrm{U}(-180{,}180) + w_{rm}.\,\mathrm{S}^{\mathrm{T}}_{\mathrm{i}=1;\mathrm{i}\neq\mathrm{t}}\left[\mathrm{G}\left(\varepsilon_s;\mu_r+\varepsilon_{i,t}+\beta_i,\sigma_r\right)\right]\}, \quad (12)$$

where the first two terms represent the same Gaussian and Uniform distributions as in model SP2_R and the third term represents errors stemming from misbinding. The weights w_s, w_{rm} and $(1-w_r-w_{rm})$ represent the *intake* of retinotopic processing (with accuracy μ_r and precision $1/\sigma_r$),

misbinding rate, and guess rate, respectively. The mean of the first Gaussian is shifted from the origin by an angle β determined by equation (6).

Models SP3c_SR and SP3r_SR: *Spatiotopic Gaussian + Retinotopic Gaussian + Uniform + Spatiotopic Misbinding Gaussian + Retinotopic Misbinding Gaussian*

These two models are represented by the following equation:

$$\begin{aligned}\mathrm{CDF}(\varepsilon_s) = \mathrm{CDF}\{&w_s.\,\mathrm{G}(\varepsilon_s;\mu_s,\sigma_s) + w_r.\,\mathrm{G}(\varepsilon_s;\mu_r+\beta,\sigma_r)\\ &+ (1-w_s-w_r-w_{sm}-w_{rm}).\,\mathrm{U}(-180,180)\\ &+ \mathrm{S}^{\mathrm{T}}_{\mathrm{i}=1;\mathrm{i}\neq\mathrm{t}}[w_{sm}.\,\mathrm{G}(\varepsilon_s;\mu_s+\varepsilon_{i,t},\sigma_s) + w_{rm}.\,\mathrm{G}(\varepsilon_s;\mu_r+\varepsilon_{i,t}+\beta_j,\sigma_t)]\}\ \},\end{aligned} \tag{13}$$

where the first three terms are the same spatiotopic Gaussian, retinotopic Gaussian and the Uniform distributions as in model SP2_SR, and the last two terms represent errors stemming from misbinding reports. The selection operator $S^{T}_{i=1;i\neq t}[.]$ determines from the set of (*T-1*) non-cued objects the misbinding item. Again, this can be either the '*closest cued feature'* item (model SP3c_SR) or the '*closest reported feature*' item (model SP3r_SR). Similar to the selected target, this misbinding item also produces a spatiotopic (fourth term) and a retinotopic (fifth term) Gaussian.

RESULTS

Eye tracking data

In our experiments, observers were required to follow eye-movement instructions while paying sufficient attention to the stimuli. Too many or too frequent invalid fixations/SPEMs in a block might lead to unreliable data because observers would then put most of their effort into the task of gaze control. Therefore, we only accepted blocks with the proportion of valid trials >=50% (See Methods for validity criteria in each condition). That is, a block was excluded if more than 56 trials were needed to obtain 28 valid trials. However; as shown below, we obtained a much higher proportion of valid trials on average. In addition, when an observer had 5 trials rejected in succession during a block of trials, we assumed the eye tracker did not hold calibration, or more likely, the calibration itself was inaccurate, due presumably to head or body movements. When this happened part way during a run, we paused the experiment to adjust and recalibrate the eye tracker and then resumed from where the run was paused. We allowed two such interruptions per block. However, we

generally discarded the block and gave observers a break if performance did not improve much after each recalibration. Finally, averaging across acceptable blocks, all observers had the proportion of valid trials >85% in fixation experiments and >70% in SPEM experiments (less than 824 and 1000 trials were needed to obtain 700 valid trials, respectively).

Figure 5 plots some examples of two-dimensional gaze traces in the SPEM condition. Also, we projected and computed the changes of eye positions along the pursuit target's direction of motion during each trial. The relative positions between eye and pursuit target are shown in Figure 6 as a function of time for some other example trials in the SPEM condition. Figures 5 and 6 suggest that, in general, the eye pursued the target with both directional and positional deviations. During the presentation of the stimuli, the eye might move in a direction not perfectly aligned with that of the pursuit target, or slightly lagging behind or running ahead of the target. To ensure accuracy, our approach for the decomposition of spatiotopic and retinotopic components shown in Figure 4 was therefore performed based on the *actual* eye-velocity vector instead of that of the pursuit target. However, the use of theoretical (i.e., pursuit target) velocity also produced very similar results (see Supplemental Information). For each trial, we fit a line to the last 200-ms part of eye movement trajectory during which the stimuli were presented, and calculated the actual direction of pursuit according to the slope of the line. The magnitude of the eye velocity vector was taken as the mean velocity over the critical period that had been calculated when considering pursuit gain (see Criteria for a valid smooth pursuit trial).

----- insert Figure 5 here -----

----- insert Figure 6 here -----

In Figure 7, the green line shows the trace of eye velocity on an example trial. Velocity was computed by digital differentiation of eye position in the direction of target motion after every 10 ms (display sampling frequency=100 Hz). To reduce noise, we used a low-pass filter with a cutoff frequency of 20 Hz (Butterworth, order = 10). The filtered trace is in blue. As mentioned earlier, averaged velocity (and that for either its horizontal or vertical component, neither of which is shown here) during the last 300-ms period had to fall in the range [0.7, 1.3] of target velocity (grey shaded area; target velocity = 5 deg/s). The black line shows the average of filtered traces obtained from 100

randomly selected trials. In general, there is a gradual drop of eye velocity in the critical pursuit interval, which can be explained by the observer's anticipation of when and where the target stops moving (Robinson et al., 1986). However, the requirement for pursuit gain in this interval is still guaranteed.

----- insert Figure 7 here -----

Overall performance

Experiments 1a and 2a: Stimulus Encoding

Figure 8 plots error magnitude ($|\varepsilon|$; right Y-axes) and transformed performance ($TP = 1 - \frac{|\varepsilon|}{180}$; left Y-axes) as a function of set size for the two eye movement conditions: (1) Fixation: Experiment 1a, left panel; and (2) SPEM: Experiment 2a, right panel. The transformation metric *TP* is defined in the same way as in our previous studies (Shooner et al., 2010; Öğmen et al., 2013; Huynh et al., 2015). *TP* can take on any value in the range [0,1], in which the values of 1 and 0.5 correspond to perfect and chance levels of performance, respectively. Since stimulus motion is different according to spatiotopic and retinotopic coordinates in the SPEM condition, we consider SPEM performance measured in each coordinate system separately. We first show here spatiotopic performance ($\varepsilon = \varepsilon_s$ in Figure 4). A two-way repeated-measures ANOVA with Huynh-Feldt correction for sphericity shows a non-significant main effect of *eye movement* (fixation vs. SPEM-spatiotopic: F(1,3)=1.179, p=0.357), a significant main effect of *set size* (F(3.776,11.329)=121.716, p<0.0001, η_p^2=0.976), and a significant interaction between the two factors (F(2.832,8.497)=4.577, p=0.036, η_p^2=0.604). This significant interaction appears to be mainly caused by the difference between fixation and SPEM-spatiotopic performance at small set sizes (see Figure 10). We conducted paired-samples t-tests, with Bonferroni correction for multiple comparisons (two-tailed, α=0.00714), to compare fixation and SPEM-spatiotopic performance at different set sizes. A significant difference was found only at a set size of 1 (t(3)=6.568, p=0.007). In fact, one observer (DHL) seems to have a different pattern of behavior than the others: This observer's fixation performance was consistently better than SPEM-spatiotopic performance for *all* set sizes, whereas for other observers fixation performance was consistently better than SPEM-spatiotopic performance

for only set size of one. However, we observed no statistical changes when observer DHL was removed from the analyses.

----- insert Figure 8 here -----

----- insert Figure 9 here -----

SPEM retinotopic performance was calculated based on the angular deviation between retinotopic and reported motion vectors ($\varepsilon = \varepsilon_r$ in figure 4). Retinotopic $|\varepsilon|$ and *TP* are shown in Figure 9 – left panel. The main effect of *eye movement* becomes significant when comparing fixation with SPEM retinotopic performance ($F(1,3)=16.595$, $p=0.027$, $\eta_p^2=0.847$), and SPEM spatiotopic with SPEM retinotopic performance ($F(1,3)=82.879$, $p=0.03$, $\eta_p^2=0.965$). In both cases, the main effect of *set size* and the interaction between *eye movement* and *set size* are significant. A one-way repeated-measures ANOVA of retinotopic SPEM performance also returns a significant effect of *set size* ($F(6,18)=20.968$, $p<0.0001$, $\eta_p^2=0.875$).

----- insert Figure 10 here -----

Fixation, SPEM-spatiotopic and SPEM-retinotopic performance averaged across observers are shown in Figure 10. Compared with a similar condition in our previous study (Huynh et al., 2015: Figure 2, middle panel, blue line), performance observed in both the fixation and SPEM (spatiotopic or retinotopic *TP*) conditions is worse[2]. This is predictable because it is likely that, when observers were required to fixate or pursue a target in the present experiment[3], more attention was drawn towards the target and less attention was distributed among the moving stimuli (Intriligator & Cavanagh, 2001). However, the progressive decay of performance with increasing set size, which indicates an early bottleneck of motion processing at the encoding stage, is consistent with our previous findings (Öğmen et al., 2013; Huynh et al., 2015).

[2] One observer (DHL) participated in both studies. His performance is only worse in the SPEM condition. There is no clear difference in his performance between the fixation condition and the Huynh et al. study (see Figure S1.1-middle).

[3] In the previous experiment, although we encouraged observers to maintain their eyes at the center of the screen during each trial in order to pay as equal attention as possible to all objects, fixation was not strictly required.

Superior performance found during pursuit in spatiotopic coordinates, compared with that in retinotopic coordinates, indicates that spatiotopic encoding dominates and/or has higher precision compared to retinotopic processing. To roughly assess the relative contribution of each component, let us consider the extreme case in which we assume motion is encoded only in a spatiotopic reference frame. If there were no noise, guessing, or non-target misreporting in observers' responses, spatiotopic performance is expected to be perfect (*TP*=1.0) whereas retinotopic performance is at some lower level, which can be calculated based on the average difference between spatiotopic and retinotopic directions of motion (β in Figure 4). As shown in Figure 9 – right panel, this level of performance is higher than chance (mean~=0.75). Because β does not depend on set size or on the actual response of the observers, we observe, as expected, a performance level that is independent of set size (F(1,3)=9.865, p=0.052, η_p^2=0.767)[4]. Comparing the left and right panels of Figure 9, one observes that performance calculated according to the retinotopic reference frame is higher than what one would expect from the case with perfect spatiotopic encoding only for set size 1 (t(3)=10.459, p=0.002, with α=0.007 with Bonferroni correction). Hence, we can state that for set size 1, it is necessary to add the retinotopic reference frame contribution to that of the spatiotopic reference frame to explain the overall performance. On the other hand, we found that performance expressed in terms of a spatiotopic reference frame is not significantly different than overall performance for set sizes 3 and above. Taken together, our results suggest that, at the stimulus encoding stage, motion stimuli are encoded mainly in a spatiotopic reference frame with a minor contribution from the retinotopic reference frame in the special case of a single target in motion. Inspection of Figure 10 also shows that for large set sizes (8-12) the difference between reference frames vanish. Previously, we proposed a "leaky-flask" model of information processing capacity, which states that significant capacity limits exist prior to memory stages (Öğmen et al., 2013; Huynh et al., 2015). Within the context of this model, we can speculate that at large set sizes, observers start to encode the motion direction of stimuli in more abstract terms such as "moving towards upper right corner", rather than metric encoding in a specific reference frame. Whereas "moving towards upper

[4] It is important to note that is distributed non-uniformly on the interval [-180, +180] across trials. This is because the spatiotopic and retinotopic components are not independent but systematically correlated. The directions of motion for the pursuit target and stimuli were randomly chosen, hence their difference (in Figure 4) is random. However, unless is sufficiently small and eye velocity is bigger than spatiotopic velocity, the value of is in general smaller than 90 deg (chance level). The same logic holds if one assumes motion is encoded only in retinotopic coordinates. In such a case, perfect responses would produce a retinotopic *TP* of 1.0 and a spatiotopic *TP* the same as retinotopic *TP* (Figure 9 – right panel) when spatiotopic encoding is assumed.

right corner" may be considered as being based on a spatiotopic reference frame, the key point is that it is a *non-metric* encoding (there is no explicit quantitative measure of angle). Given that spatiotopic and retinotopic reference frames are correlated, one would expect the difference between the two reference frames to vanish, even though performance is still better than chance.

Similar observations have been made in previous studies of ensemble coding. Corbett and Melcher (2014) had observers adapting to mean-size of dots of various sizes and examined the reference frame used for the resulting size aftereffect. The mean-size aftereffects (a test dot appeared larger following adaptation to small dots and smaller after adaptation to large dots) were seen when the test dot was presented at the appropriate retinotopic or spatiotopic location relative to the adapted region, or even at locations that were neither retintopic or spatiotopic, but were within the adapted hemifield, suggesting that multiple reference frames are used in the encoding of mean-size. Corbett and Melcher suggest that ensemble representations may be available at multiple levels across the hierarchy of visual processing and these representations efficiently represent abstract, global properties. Even though our study did not explicitly ask observers to report ensemble properties of the stimuli, the use of multiple frames and the abstract encoding of motion may be indicative of the implicit intrusion of ensemble representations for the larger set-sizes (see Brady & Alvarez, 2015). However, care must be exercised when extrapolating across feature domains with regard to principles of ensemble coding (Hubert-Wallander & Boynton, 2015).

Experiments 1b and 2b: Sensory memory and VSTM

Figure 11 plots fixation (left), SPEM spatiotopic (middle), and SPEM retinotopic (right) performance as a function of cue delay. Average data are shown in Figure 12. A two-way repeated-measures ANOVA with Huynh-Feldt correction for sphericity shows a significant main effect of *eye movement* (fixation vs. SPEM spatiotopic: $F(1,3)=35.583$, $p=0.009$, $\eta_p^2=0.922$), a significant main effect of *cue-delay* ($F(6,18)=8.948$, $p<0.0001$, $\eta_p^2=0.749$), and a non-significant interaction between the two factors ($F(3.135,9.405)=0.762$, $p=0.547$, $\eta_p^2=0.203$). Given the insignificant difference between fixation and SPEM spatiotopic performance observed at the encoding stage for set size 6 in Experiments 1a and 2a, we carried out pairwise comparisons to examine whether the significant effect of eye movement we just found exists across all three processing stages (encoding, sensory memory, and VSTM). We grouped the data according to corresponding groups of cue delay samples and ran paired-samples t-tests to compare fixation and SPEM spatiotopic *TP*s for each group.

Results from a similar experimental condition in our previous study suggest that the two samples at 1 s and 3 s mainly involve the operation of VSTM whereas shorter non-zero-delay samples reflect sensory memory (see Huynh et al. (2015): Table 2 – row 3). This can be confirmed in the current study by inspection of the average fixation and SPEM spatiotopic performance in Figure 12, which conform closely to an exponential decay function. Using the same method as in Öğmen et al. (2013) to demarcate sensory and VSTM, we fit observers' average performance in each eye movement condition to an exponential of the form $A+Be^{t/\tau}$ and obtained time-constants (τ) of 292 and 154 ms for the fixation and SPEM (spatiotopic) cases, respectively. Although performance in the latter case reaches steady-state level that represents VSTM earlier (3τ=462 ms, which precedes the sample at 500 ms), it is more reasonable to keep the demarcation between the two memory systems consistent across eye movement conditions and in the same way as in Huynh et al. (2015). Three paired-samples t-tests (two-tailed, α=0.0167) yield a significant difference between fixation and SPEM spatiotopic *TP*s at the sensory memory stage (t(3)=10.052, p=0.002), but not at the encoding (t(3)=3.490, p=0.040) or VSTM (t(3)=3.460, p=0.041) stages. The insignificant difference at the encoding stage (zero cue delay) is consistent with the finding in Experiments 1a and 2a. We also find that spatiotopic performance is significantly better than retinotopic performance (F(1,3)=41.217, p=0.008, η_p^2=0.932). However, pairwise comparisons (two-tailed, α=0.0167) show that the difference is only significant at the encoding stage (t(3)=6.029, p=0.009). The insignificant difference found at the two memory stages is not necessarily a hallmark of equivalent contributions of the spatiotopic and retinotopic representations. The drop of spatiotopic performance over time due to increasing guessing and misreporting responses might be the main cause because a one-way repeated-measures ANOVA with Huynh-Feldt correction for sphericity shows that the effect of cue delay on retinotopic performance is not significant (F(3.051,9.152)=3.575, p=0.059, η_p^2=0.544). If indeed, at set size 6 the retinotopic reference frame has no contribution to the performance, as suggested by the findings of Experiment 1, performance plotted in terms of the retinotopic reference frame may represent an overall lower baseline, independent of stimulus encoding and memory stages.

Statistical modeling

Model selection

Model selection was used to find the model or group of models that best describe the behavioral data. In the Least Squares method, the models were compared based on their adjusted R^2 values[5], a measure of their goodness of fit. The model with the highest adjusted R^2 was considered the best-performing model. Table 1 provides average values of adjusted R^2 obtained for all conditions and models. In the fixation condition, our analyses in both experiments 1a and 1b show that the three models F2, F3c, and F3r have equivalent performance, which is significantly better than that of model F1. Model F2 was selected because it contains the smallest number of free parameters. In the SPEM condition, as stated in the Data Analysis section, our models can be grouped based on two factors, i.e. uncertainty and reference frame. The former one is the same as used to formulate the models in the fixation condition, which is to consider whether a model accounts for guessing and misreporting in the observers' responses. The latter factor indicates the nature of reference systems (spatiotopic, retinotopic, or combined) associated with the encoding and retention of information assumed by each model. Consistently across experiments 1b and 2b, we find that performance is equivalent for the SP2_*, SP3c_*, and SP3r_* groups, which is significantly better than the SP1 group. Equivalent performance was also found for the spatiotopic (*_S) and combined (*_SR) groups, which is significantly better then the retinotopic (*_R) group. The result does not change when comparing the spatiotopic (*_S) and combined (*_SR) groups for each memory stage separately. Taken together, the model SP2_S was chosen for its smallest number of parameters. This finding implies that a spatiotopic model is sufficient to fully account for the variability in the observers' behavior and reinforces our speculation above that the encoding and retention of motion information is essentially spatiotopic.

Parameter estimation

We report in this section estimates for the parameters of the winning model in each condition. Figure 13 plots averaged values for *intake* (along with *guess rate* = $1 - $ *intake*) and *precision* obtained in experiments 1a (fixation) and 2a (SPEM) as a function of set size. As mentioned in the Data analysis section, *intake* (w in model F2 or w_s in model SP2_S) and *precision* ($1/\sigma$ in model F2 or $1/\sigma_s$ in model SP2_S) respectively represent the quantitative and qualitative aspects of

[5] The following equation was used to compute adjusted R^2:

$$Adjusted\ R^2 = 1 - (1 - R^2)\frac{n-1}{n-p-1}$$

where *n* is the sample size and *p* is the number of independent variables (parameters) in the model.

performance. We observe a linear drop of intake with increasing set size in both the fixation and SPEM conditions, and there is no significant difference between the two conditions. The relationship between precision and set size is non-linear with a big difference between the two conditions at a set size of 1. However, this difference in precision gradually vanishes at larger set sizes, which explains the superior fixation performance only at set size of 1 we found earlier. It should be noted here that we excluded this set size when comparing our models (see table 1) because models that contain misbinding components are not applicable when there is only a single object presented. For the set size of 1, model comparison was run separately, and the winning models remain the same as those for the other cases (model F2 in the fixation condition and the spatiotopic model SP2_S in the SPEM condition). This suggests that the special finding at a set size of 1 does not come from any apparent influence of retinotopic processing but, presumably, from a higher depletion of attentional resources caused by oculomotor control in the SPEM condition compared with that in the fixation condition. The increase of uncertainty when having larger numbers of objects might have rendered precision in both the fixation and SPEM conditions to drop to a level at which the difference in attentional deployment was no longer noticeable.

Figure 14 plots averaged values for *intake* and *precision* obtained in Experiments 1b (fixation) and 2b (SPEM) as a function of cue-delay. Recall that these two experiments consistently used a set size of 6 while varying cue-delay to examine the sensory and VSTM stages of information processing. Given a bottleneck of processing at the encoding stage demonstrated by the degradation of performance with increasing set size in Experiments 1a and 2a, analyzing the extent to which the degradation of performance changes over time provides information about the distribution of information loss across different processing stages. According to our previous findings (Öğmen et al., 2013; Huynh et al., 2015) and preliminary data for the present experiments (not shown), performance at a set size of 1 is relatively stable over the interval 0-3s. In Figure 14, this is represented by the horizontal dashed lines extended from the single data points at zero cue delay (obtained in the single object condition in Experiments 1a and 2a). The pattern of results for both intake and precision is similar in the fixation and SPEM conditions and is consistent with our findings in Öğmen et al. study and with the case of cueing position and reporting direction of motion in Huynh et al. (2015). That is, we find that most of the decay in precision occurs at the encoding stage whereas the decay in intake is more gradual. A one-way repeated-measures ANOVA of precision shows no effect of cue-delay in either the fixation or SPEM conditions. For intake,

approximately half of the decay is at the encoding stage. These findings are in agreement with our Leaky Flask model proposed in Öğmen et al. (2013).

GENERAL DISCUSSION

This study aimed to investigate the reference frame used in perceptual encoding and storage of visual motion information. In our experiments, observers viewed multiple moving objects and reported the direction of motion of a randomly selected item. The task was performed while the observers were either fixating a stationary point or smoothly pursuing a target moving at a constant velocity. In the fixation condition, the non-retinotopic component of a motion stimulus is fully confounded with its retinotopic component. In the SPEM condition, with eyes moving from one position to another, the two components can be dissociated. Using a vector decomposition technique, we were able to compute performance during SPEM with respect to spatiotopic (non-retinotopic) and retinotopic motion components and compare them with performance during fixation, which serves as the baseline. We also used several hypothetical models to quantitatively and qualitatively simulate different aspects, including the possible involvement of each reference frame, of the observers' behaviors.

For the stimulus encoding stage, which precedes memory, we found that the reference frame depends on stimulus set-size. For the special case where the stimulus consists of a single moving target, the spatiotopic reference frame had the most significant contribution with some additional contribution from the retinotopic reference frame. To a close approximation, the relative contributions of the two reference frames can be quantified based on the two extreme cases we discussed earlier for a set size of 1. Average performance at a set size of 1 in the fixation condition (approximately 0.96; Figure 8 – left panel) can be considered as SPEM spatiotopic performance if motion is assumed to be encoded exclusively in a spatiotopic reference frame. On the other hand, if no spatiotopic reference frame is used, SPEM spatiotopic performance is expected to be about 0.75 (Figure 9 – right panel). There is a total drop of 0.21 in performance between the two extremes. In reality, we obtained a SPEM spatiotopic performance of 0.92. This corresponds to a drop of 0.04, approximately one fifth of the total drop. Therefore, the contribution ratio of spatiotopic to

retinotopic reference frames is roughly 4:1. The contribution of both retinotopic and spatiotopic reference frames for isolated moving targets is in agreement with previous studies (Souman et al., 2005a, 2005b, 2006a; Swanston & Wade, 1988). Although the relative contributions of the reference frames were not provided in these studies, some comparisons can be made between our and their data. To account for errors in motion perception during SPEMs, these studies applied a linear model (von Holst, 1954) in which the perceived head-centric velocity **h'** of a stimulus is viewed as a weighted sum of its retinal image velocity **r** and eye velocity **e,** i.e. $\mathbf{h'} = \rho.\mathbf{r} + \varepsilon.\mathbf{e}$ (for alternative models, see Wertheim, 1994; Freeman, 2001; Turano & Massof, 2001). To compute **h'**, the visual system obtains estimates of the actual signals **r** and **e**. The weights ρ and ε in the model describes the gains associated with these estimates. The deviation of the perceived direction **h'** from the physical direction **h** depends on the gain ratio ε/ρ. During SPEM, the direction of **h'** is typically biased towards the direction of **r,** which can be explained by a gain ratio that is smaller than one. The smaller the gain ratio is, the larger the bias becomes. In case that $\varepsilon = \rho = 1$, $\mathbf{h'} = \mathbf{h} = \mathbf{r} + \mathbf{e}$. For example, Souman et al. (2005b) measured the perceived motion direction of a stimulus moving at various angles (0-360°) relative to the pursuit direction. The perceived direction data were fit to the linear model above with the gain ratio ε/ρ being the only free parameter, which was assumed to be fixed across stimulus directions. Souman et al. found a high degree of fit ($R^2 \sim 90\%$) for most observers. They obtained relatively low estimates for ε/ρ, and this ratio decreased with increasing stimulus speed (3°/s: mean=0.53, standard deviation=0.12; 8°/s: mean=0.21, standard deviation=0.1; calculations are based on data in Table 1, Souman et al., 2005b). One can predict that, if the same stimulus speed as in our study (5°/s) were used, the mean gain ratio would be smaller than 0.53 and greater than 0.21. For comparison, we applied the same linear model and simulation on our data for the set size of 1 in Experiment 2a and obtained a value of ε/ρ that is much higher than predicted (ε/ρ = 0.80, 0.63, 0.77, 0.63 for observers TTN, TAN, QVP, DHL, respectively; mean=0.71, standard deviation=0.09). This suggests that our observers generally made smaller errors in judging the direction of motion of the stimulus, and one can conclude that the data in the Souman et al. study show a larger contribution of the retinotopic reference frame compared to our finding. Let us note, however, that the estimation of contribution ratio we obtained earlier is only meaningful on average data, i.e. performance for different deviations between the pursuit target and the direction of stimulus motion is averaged. The reason for this is that, given the visual system uses some fixed gain ratio for different stimulus directions, the magnitude of errors of the judged motion direction

during SPEM typically depends on the angle between the stimulus and pursuit target motion directions. With the exception of Souman et al. (2005b), most previous studies of motion perception during SPEM (Becklen et al., 1984; Wallach et al., 1985; Souman et al., 2005a; Souman et al., 2006a; Souman et al., 2006b; Swanston & Wade, 1988) focus on horizontal and vertical movements of stimuli and the pursuit target. Therefore, it is hard to quantitatively compare those with our study. However, one potentially important factor that might amplify the contribution of retinotopic encoding in all of these studies is that their experiments were performed in total darkness, with only the stimulus and the pursuit target visible. This would have eliminated the stationary background and the display as usable spatiotopic reference frames. The use of a relatively short stimulus presentation duration (200 ms) in our experiments is unlikely to be a reason for the weak effect of retinotopic reference frame we observed. It has been shown that decreasing the stimulus presentation duration increases errors (biases) in the perceived motion direction during pursuit (Mack & Herman, 1978; De Graaf & Wertheim 1988; Souman et al., 2005a). Therefore, the shorter the presentation duration, the stronger the expected contribution of the retinotopic reference frame. Furthermore, as shown in Souman et al. (2005a), the effect of stimulus duration is negligible for low stimulus velocities, such as that used in our experiments (5°/s).

When the number of items in the stimulus increased, the spatiotopic reference frame alone was able to account for the overall performance. Finally, when the number of items became large, the distinction between reference frames vanished. We interpret this finding as a switch to a more abstract encoding of motion direction, such as "towards lower right", instead of a metric encoding within a specific reference frame. Our earlier studies showed significant capacity limits already at the stimulus encoding stage, leading to the "leaky flask model" (see Öğmen et al., 2013 - Figure 10). The results of this study are also in agreement with the leaky flask model. When the stimulus set-size increases, due to capacity limits, it may not be possible for the visual system to encode all directions of motion according to a reference-frame metric. One strategy would be then to switch to a more descriptive non-metric encoding. Another way the visual system can handle the complexity of a stimulus comprising multiple moving targets (large set-size) is through Gestalt grouping mechanisms. For example, the point lights placed on a person in the biological motion paradigm (Johansson, 1973) creates a very complex stimulus; however, by grouping these points into a meaningful Gestalt (Yantis, 1992), the visual system is capable of computing a common reference frame, which can be used to simplify the *relative* motions of various point lights. Several studies

showed that when the stimulus allows grouping of parts, motion groupings based non-retinotopic reference frames (relative motion) account for perceived direction of motion (Duncker, 1938; Johansson, 1973; Boi et al., 2009; Noory et al., 2015; Agaoglu et al., 2015a,b). In fact, Agaoglu et al. (2015b) quantified the contributions of retinotopic, spatiotopic, and relative-motion reference frames and showed that relative motion dominated both during fixation and SPEM, with a contribution more than 80% when the distance between the stimuli was 2 degrees. The dominance of the relative motion decreased with the distance between stimuli; however, for separations as large as 11 deg, the contribution of relative motion was still substantial (60%). Each disk in our experiments here had an independently and randomly chosen direction and hence our stimulus was not conducive to this type of (relative) non-retinotopic reference frame. Instead, the non-retinotopic reference frame was presumably a screen-based (spatiotopic) reference frame.

SPEM not only causes biases in motion perception but also leads to mislocalizations of stimuli (Mita et al., 1950; Ward, 1976; Brenner et al., 2001; van Beers et al., 2001; Rotman et al., 2005; Souman et al., 2006a). Importantly, both the magnitude and the direction of mislocalization when pursuit is towards the stimulus are different from those when pursuit is away from the stimulus (Mitrani & Dimitrov, 1982; Mateeff & Hohnsbein, 1988; Mateeff et al., 1991; Rotman et al., 2004). Also, mislocalization is more pronounced for stimuli that are more distant from the pursuit path (Souman et al., 2006a). We expect that these asymmetric effects on localization also apply to direction-of-motion perception, although the direct physical relationship between location and motion may not exist in perceptual terms (Snowden, 1994; Souman et al., 2006a). It should be noted that, because the cued target's location and motion direction, as well as the direction of pursuit were chosen randomly across trials, these asymmetries should be averaged out and are not considered in our data.

In terms of memory, we found that performance expressed in terms of a retinotopic reference frame did not depend on cue delay, suggesting that the retinotopic reference frame was not used during memory storage. The difference between fixation and SPEM performance in terms of a spatiotopic reference frame was not significant at stimulus encoding and VSTM stages, but it was significant for the sensory memory stage. As mentioned before, whereas earlier studies found that sensory memory uses a retinotopic reference frame, more recent studies using sequential metacontrast and Ternus-Pikler displays indicate that sensory memory can also use a motion-based non-retinotopic reference frame (Ogmen et al., 2006; Otto et al., 2006; Scharnowski et al., 2007;

Noory et al, 2015). Because performance in sensory memory in terms of a spatiotopic reference frame was superior to that in terms of a retinotopic reference frame and because spatiotopic performance showed the typical exponential delay observed in sensory memory (Figure 12), we conclude that our findings here are in agreement with the existence of a non-retinotopic sensory memory component.

When set size was large (8-12 objects) motion performance expressed in a spatiotopic reference-frame in the SPEM condition was comparable to that expressed in a retinotopic reference-frame. Similar findings have been reported in a study that investigated ensemble coding of mean-size using adaption aftereffects and found that adaptation to mean size occurred in multiple reference-frames, that included retinotopic and spatiotopic frames, among others (Corbett & Melcher, 2014). The study also reported an abstract representation of mean size, similar to the abstract representation of motion direction we find in the current study. While the current study did not specifically investigate ensemble encoding of motion, the influence of ensemble coding, for the larger set-sizes we investigated, cannot be ruled out (see Brady & Alvarez, 2015). Corbett and Melcher (2014) interpreted their findings to suggest that mean-size is represented in multiple levels in the visual hierarchy, and this is important for perceptual stability. It is likely that, for large set-sizes, motion direction too is represented in multiple reference-frames at different levels in the visual hierarchy, facilitating perceptual stability. However, how principles of ensemble coding in one perceptual task generalize to another is an open question (Hubert-Wallander & Boynton, 2015).

In summary, our results along with other recent findings suggest that, whereas a retinotopic reference frame may be useful for controlling eye-movements, non-retinotopic reference frames may characterize perception and memory. Furthermore, the use of a non-retinotopic reference frame appears to be capacity limited. In the case of complex stimuli (large set-size), the visual system may use perceptual grouping or summary statistics or ensemble representations in order to simplify the complexity of stimuli (as in studies involving mean-size, biological motion, or Ternus-Pikler displays), or resort to a non-metric abstract coding of motion information.

REFERENCES

Agaoglu, M. N., Herzog, M. H., & Öğmen, H. (2015a). Field-like interactions between motion-based reference frames. *Attention, Perception & Psychophysics*, 77: 2082-2097.

Agaoglu, M. N., Herzog, M. H., & Öğmen, H. (2015b). The effective reference frame in perceptual judgments of motion direction. *Vision Research*, 107: 101-112.

Andersen, R. A., Snyder, L. H., Li, C. S., & Stricanne, B. (1993). Coordinate transformations in the representation of spatial information. *Current Opinion in Neurobiologyl*, 3: 171–176.

Ariely, D. (2001). Seeing sets: Representation by statistical properties. *Psychological Science*, 12: 157-162.

Atkinson, R. C., & Shiffrin, R. M. (1968). Human memory: A proposed system and its control processes. In Spence, K. W., & Spence, J. T. *The psychology of learning and motivation* (Volume 2). New York: Academic Press. pp. 89–195.

Baddeley, A .D., & Hitch, G. (1974). Working memory. In G.H. Bower (Ed.), *The psychology of learning and motivation: Advances in research and theory* (Vol. 8, pp. 47–89). New York: Academic Press.

Baker, J. T., Harper, T. M., & Snyder, L. H. (2003). Spatial memory following shifts of gaze. I. Saccades to memorized world-fixed and gaze-fixed targets. *Journal of Neurophysiology*, 89: 2564–2576.

Bauer, B. (2015). A selective summary of visual averaging research and issues up to 2000. *Journal of Vision,* 15(4):14, 1-15.

Bays, P.M., Catalao, R.F.G., & Husain, M. (2009). The precision of visual working memory is set by allocation of a shared resource. *Journal of Vision*, 9(10), Article Number: 7.

Becklen, R., Wallach, H., Nitzberg, D. (1984). A limitation of position constancy. *Journal of Experimental Psychology: Human Perception and Performance,* 10: 713–723.

Boi, M., Öğmen, H., Krummenacher, J., Otto, T. U., & Herzog, M. H. (2009). A (fascinating) litmus

test for human retino- vs. non-retinotopic processing, *Journal of Vision*, 9(13):5, 1-11.

Brady, T.M., & Alvarez, G.A. (2015). No evidence for a fixed object limit in working memory: Spatial ensemble representations inflate estimates of working memory capacity for complex objects. *Journal of Experimental Psychology: Learning, Memory, and Cognition,* 41(3): 921-929.

Braun, D. I., Schütz, A. C., Gegenfurtner, K. R. (2010). Localization of speed differences of context stimuli during fixation and smooth pursuit eye movements. *Vision Research,* 50:2740-2749.

Bremner, A. J., Bryant, P. E., & Mareschal, D. (2005). Object-centred spatial reference in 4-month-old infants. *Infant Behaviour and Development*, 29: 1-10.

Brenner, E., Smeets, J., & Van den Berg, A. V. (2001) Smooth eye movements and spatial localisation. *Vision Research* 41: 2253–2259.

Bridgeman, B. (1995). A review of the role of efference copy in sensory and oculomotor control systems. *Annals of Biomedical Engineering*, 23: 409–422.

Bridgeman, B., Van der Heijden, A. H., & Velichkovsky, B. M. (1994). A theory of visual stability across saccadic eye movements. *Behavioral and Brain Sciences*, 17: 247–258.

Burr, D. (1980). Motion smear. *Nature,* 284(5752): 164-165.

Burr, D. C., & Morrone, M. C. (2011). Spatiotopic coding and remapping in humans. *Philosophical Transactions of the Royal Society of London B,* 366 (1564): 504–515.

Burr, D. C., & Morrone, M. C. (2012). Constructing stable spatial maps of the world. *Perception*, 41 (11): 1355–1372.

Buswell, G. T. (1935). *How people look at pictures*. Chicago: University of Chicago Press.

Cant, J.S., Sun, S.Z., & Xu, Y. (2015). Distinct cognitive mechanisms involved in the processing of single objects and object ensembles. *Journal of Vision,* 15(4):12, 1-21.

Cavanagh, P., Hunt, A. R., Afraz A., & Rolfs M. (2010). Visual stability based on remapping of attention pointers. *Trends in Cognitive Sciences,* 14 (4): 147–153.

Chen, S., Bedell, H. E., & Öğmen H. (1995). A target in real motion appears blurred in the absence of other proximal moving targets. *Vision Research*, 35: 2315–2328.

Corbett, J.E., & Melcher, D. (2014). Characterizing ensemble statistics: mean size is represented across multiple reference frames. *Attention, Perception, & Psychophysics,* 76: 746-758.

de Fockert, J., & Wolfenstein, C. (2009). Rapid extraction of mean identity from sets of faces. *Quarterly Journal of Experimental Psychology,* 62, 1716-1722.

De Graaf, B., & Wertheim, A. H. (1988). The perception of object-motion during smooth-pursuit eye movements: adjacency is not a factor contributing to the Filehne illusion. *Vision Research*, 28:497–502.

Dempster, A.P., Laird, N.M., & Rubin, D.B. (1977). Maximum likelihood from incomplete data via the EM algorithm. *Journal of the Royal Statistical Society, Series B,* 39 (1): 1–38.

Dixon, P., & Di Lollo, V. (1994). Beyond visible persistence: An alternative account of temporal integration and segregation in visual processing. *Cognitive Psychology*, 26: 33-63.

Duncker, K. (1938). *Induced motion. In W. D. Ellis (Ed.), A sourcebook of Gestalt psychology*. London: Routledge & Kegan Paul. Original work published in German, 1929.

Engel, S. A. (1994). fMRI of human visual cortex. *Nature*, 370(6485): 106-106.

Festinger, L., Sedgwick, H. A., & Holtzman, J. D. (1976). Visual perception during smooth pursuit eye movement. *Vision Research*, 16: 1377-1386.

Freeman, T. C. A. (2001). Transducer models of head-centred motion perception. *Vision Research*, 41: 2741–2755.

Gardner, J. L., Merriam, E. P., Movshon, J. A., & Heeger, D. J. (2008). Maps of visual space in human occipital cortex are retinotopic, not spatiotopic. *Journal of Neuroscience*, 28(15): 3988-3999.

Gibaldi, A., Canessa, A., & Sabatini, S. P. (2016). Visuomotor behavior of dominant and non-dominant eye in 3D visual exploration. *ECVP Abstracts*.

Golomb, J. D., & Kanwisher, N. (2012). Retinotopic memory is more precise than spatiotopic memory. *Proceedings of the National Academy of Sciences of the United States of America*. 109(5): 1796-1801.

Haber, R. N. (1983). The impending demise of the icon: A critique of the concept of iconic storage in visual information processing. *Behavioral and Brain Sciences,* 6: 1-54.

Haberman, J., & Whitney, D. (2007). Rapid extraction of mean emotion and gender from sets of faces. *Current Biology*, 17, R751-R753.

Horowitz, T.S. & Cohen, M.A. (2010). Direction information in multiple object tracking is limited by a graded resource. *Attention, Perception, & Psychophysics*, 72: 1765-1775.

Howe, P. D. L., Pinto, Y., & Horowitz, T. S. (2010). The coordinate systems used in visual tracking. *Vision Research*, 50: 2375-2380.

Hubert-Wallander, B., & Boynton, G.M. (2015). Not all summary statistics are made equal: Evidence from extracting summaries over time. *Journal of Vision*, 15(4):5, 1-12.

Huynh, D., Tripathy, S. P., Bedell, H. E., & Öğmen, H. (2015). Stream specificity and asymmetries in feature binding and content-addressable access in visual encoding and memory. *Journal of Vision*, 15(13):14, 1–32.

Intriligator, J., & Cavanagh, P. (2001). Spatial resolution of visual attention. *Cognitive Psychology*, 43(3): 171-216.

Irwin, D.E., Brown, J.S., & Sun, J.S. (1988). Visual masking and visual integration across saccadic eye-movements. *Journal of Experimental Psychology-General*, 117(3): 276-287.

Irwin, D.E., Yantis, S., Jonides, J. (1983). Evidence against visual integration across saccadic eye-movements. *Perception & Psychophysics*, 34(1): 49-57.

Jancke, D., Chavane, F., Naaman, S., & Grinvald, A. (1987). Imaging cortical correlates of illusion in early visual cortex. *Journal Of Experimental Psychology-Human Perception And Performance*, 13(1): 140-145.

Johansson, G. (1973). Visual perception of biological motion and a model for its analysis. *Perception and Psychophysics*, 14: 201–211.

Jonides, J., Irwin, D.E., & Yanstis, S. (1983). Failure to integrate information from successive fixations. *Science,* 222(4620): 188-188.

Levi, D.M., & Tripathy, S.P. (2006). Is the ability to identify deviations in multiple trajectories compromised by amblyopia? *Journal of Vision*, 6(12): 1367-1379.

Mack, A. (1986). Perceptual aspects of motion in the frontal plane. In K. R. Boff, L. Kaufman, & J. P. Thomas (Eds.). *Handbook of perception and human performance* (Vol. I, chap. 17, pp. 1-38). New York: Wiley.

Mack, A., & Herman, E. (1978). The loss of position constancy during pursuit eye movements. *Vision Research,* 18: 55–62.

Mateeff, S. (1980). Visual perception of movement patterns during smooth eye tracking. *Acta Physiologica et Pharmacologica Bulgarica*, 6: 82-89.

Mateeff, S., & Hohnsbein, J. (1988). Perceptual latencies are shorter for motion towards the fovea than for motion away. *Vision Research*, 28: 711–719.

Mateeff, S., Yakimoff, N., Hohnsbein, J., Ehrenstein, W. H., Bohdanecky, Z., & Radil, T. (1991). Selective directional sensitivity in visual motion perception. *Vision Research,* 31: 131–138.

Mays, L. E., & Sparks, D. L. (1980). Dissociation of visual and saccade-related responses in superior colliculus neurons. *Journal of Neurophysiology*, 43: 207-232.

McKenzie, A., & Lisberger, S. G. (1986). Properties of signals that determine the amplitude and direction of saccadic eye movements in monkeys. *Journal of Neurophysioly,* 56: 196–207.

Melcher, D., & Colby, C. L. (2008). Trans-saccadic perception. *Trends in Cognitive Sciences*, 12: 466–473.

Melcher, D., & Fracasso, A. (2012). Remapping of the line motion illusion across eye movements. *Experimental Brain Research,* 218: 503-514.

Melcher, D., & Morrone, M. C. (2015). Non-retinotopic visual processing in the brain. *Visual Neuroscience*, 32, E017.

Miles, W. R. (1929). Ocular dominance demonstrated by unconscious sighting. Ocular dominance demonstrated by unconscious sighting. *Journal of Experimental Psychology, 12*, 113-126.

Miles, W. R. (1930). Ocular dominance in human adults. *Journal of General Psychology,* 3: 412-429.

Mita, T., Hironaka, K., & Koike, I. (1950). The influence of retinal adaptation and location on the ‘‘Empfindungszeit’’. *Tohoku Journal of Experimental Medicine*, 52: 397–405.

Mitrani, L., & Dimitrov, G. (1982). Retinal location and visual localization during pursuit eye movement. *Vision Research,* 22: 1047–1051.

Narasimhan, S., Tripathy, S.P., & Barrett, B.T. (2009). Loss of positional information when tracking multiple moving dots: The role of visual memory. *Vision Research*, 49: 10–27.

Nishida, S. (2004). Motion-based analysis of spatial patterns by the human visual system. *Current Biology*, 14: 830–839.

Noory B., Herzog M. H., & Öğmen H. (2015). Spatial properties of non-retinotopic reference frames in human vision, *Vision Research*, 113: 44-54.

Norman, L.J., Heywood, C.A., & Kentridge, R.W. (2015). Direct encoding of orientation variance in the visual system. *Journal of Vision*, 15(4):3, 1-14.

Nyström, M., Andersson, R., Holmqvist, K., & van de Weijer, J. (2013). The influence of calibration method and eye physiology on eyetracking data quality, *Behavior Research Methods,* 45: 272-288.

Öğmen, H. (2007). A theory of moving form perception: Synergy between masking, perceptual grouping, and motion computation in retinotopic and non-retinotopic representations. *Advances in Cognitive Psychology*, 3: 67‑84.

Öğmen, H., Ekiz, O., Huynh, D., Tripathy, S. P., & Bedell, H. E. (2013). Bottlenecks of motion processing during a visual glance: The leaky flask model. *PLoS One.*

Öğmen, H., & Herzog, M. H. (2010). The geometry of visual perception: Retinotopic and nonretinotopic representations in the human visual system. *Proceedings of the IEEE*, 98: 479‑492.

Öğmen, H., Otto, T.U., & Herzog, M.H. (2006). Perceptual grouping induces non-retinotopic feature attribution in human vision. *Vision Research*, 46(19): 3234-3242.

Ong, W. S., Hooshvar, N., Zhang, M., & Bisley, J. W. (2009). Psychophysical evidence for spatiotopic processing in area MT in a short-term memory for motion task. *Journal of Neurophysiology*, 102: 2435–2440.

Orban de Xivry, J. J., Lefèvre, P. (2007). Saccades and pursuit: two outcomes of a single sensorimotor process. *Journal of Physiology.*, 584: 11–23.

Otto, T., Öğmen, H., & Herzog, M. H. (2006). The flight path of the phoenix: The visible trace of invisible elements in human vision. *Journal of Vision*, 6: 1079-1086.

Pertzov, Y., Avidan, G., & Zohary, E. (2011). Multiple reference frames for saccadic planning in the human parietal cortex. *Journal of Neuroscience,* 31:1059 –1068.

Pylyshyn, Z., & Storm, R. (1988). Tracking multiple independent targets: evidence for a parallel tracking mechanism. *Spatial Vision,* 3: 179-197.

Rashbass, C. (1961). The relationship between saccadic and smooth tracking eye movements. *Journal of Physiology (London),* 159: 326–38.

Rayner, K., & Pollatsek, A. (1983). Is visual information integrated across saccades? *Perception & Psychophysics*, 34(1): 39-48.

Robinson, D. A., Gordon, J. L., & Gordon, S. E. (1986). A model of the smooth pursuit eye movement system. *Biological Cybernetics*, 55: 43–57.

Rotman, G., Brenner, E., & Smeets, J. B. J. (2004). Quickly tapping targets that are flashed during smooth pursuit reveals perceptual mislocalizations. *Experimental Brain Research*, 156: 409–414.

Rotman, G., Brenner, E., & Smeets, J. B. J. (2005). Flashes are localized as if they were moving with the eyes. *Vision Research*, 45: 355–364.

Scharnowski, F., Hermens, F., Kammer, T., Öğmen, H., & Herzog, M. H. (2007). Feature fusion reveals slow and fast memories, *Journal of Cognitive Neuroscience*, 19: 632-641.

Sereno, M. I., Pitzalis, S., & Martinez, A. (2001). Mapping of contralateral space in retinotopic coordinates by a parietal cortical area in humans. *Science*, 294(5545): 1350-1354.

Shooner, C., Tripathy, S., Bedell, H., & Öğmen, H. (2010). High-capacity, transient retention of direction-of-motion information for multiple moving objects. *Journal of Vision*, 10(6):8, 1-20.

Snowden, R. J. (1994). Motion processing in the primate cerebral cortex. In: Smith AT, Snowden RJ (eds) Visual detection of motion. *Academic, London*, pp 51–83.

Souman, J. L., Hooge, I. T. C., & Wertheim, A. H., (2005a). Vertical object motion during horizontal ocular pursuit: compensation for eye movements increases with presentation duration. *Vision Research*, 45: 845-853.

Souman, J. L., Hooge, I. T. C., & Wertheim, A. H., (2005b). Perceived motion direction during smooth pursuit eye movements. *Experimental Brain Research*, 164: 376-386.

Souman, J. L., Hooge, I. T. C., & Wertheim, A. H., (2006a). Localization and motion perception during smooth pursuit eye movement. *Experimental Brain Research*, 171: 448-458.

Souman, J. L., Hooge, I. T. C., & Wertheim, A. H., (2006b). Frame of reference transformations in motion perception during smooth pursuit eye movements. *Journal of Computational Neuroscience*, 20: 61-76.

Sun, J.S., & Irwin, D.E. (1987). Retinal masking during pursuit eye-movements - implications for spatiotopic visual persistence. *Journal of Experimental Psychology-Human Perception and Performance*, 13(1): 140-145.

Swanston, M. T., & Wade, N. J. (1988). The perception of visual motion during movements of the eyes and of the head. *Perception & Psychophysics*, 43: 559-566.

Sweeny, T. D., Haroz, S., & Whitney, D. (2012). Perceiving Group Behavior: Sensitive Ensemble Coding Mechanisms for Biological Motion of Human Crowds. *Journal of Experimental Psychology: Human Perception and Performance*. 39:329-337.

Tootell, R. B. H., Hadjikhani, N. K., Vandufflel, W., Liu, A. K., Mendola, J. D., Sereno, M. I., et al. (1998). Functional analysis of primary visual cortex (V1) in humans. *Proceedings of the National Academy of Sciences of the United States of America*, 95(3): 811-817.

Tootell, R. B. H., Reppas, J. B., Kwong, K. K., Malach, R., Born, R. T., Brady, T. J., et al. (1995). Functional analysis of human MT and related visual cortical areas using magnetic-resonance-imaging. *Journal of Neuroscience*, 15(4): 3215-3230.

Tripathy, S.P., & Barrett, B.T. (2004). Severe loss of positional information when detecting deviations in multiple trajectories. *Journal of Vision*, 4(12): 1020-1043.

Tripathy, S.P., & Levi, D.M. (2008). On the effective number of tracked trajectories in amblyopic human vision. Journal of Vision, 8(4):4, 1–22, http://journalofvision. org/7/6/2/, doi:10.1167/7.6.2.

Tripathy, S.P., Narasimhan, S., & Barrett, B.T. (2007). On the effective number of tracked trajectories in normal human vision. Journal of Vision, 7(6):2, 1–18, http://journalofvision.org/7/6/2/, doi: 10.1167/7.6.2.

Turano, K. A., & Massof, R. W. (2001). Nonlinear contribution of eye velocity to motion perception. *Vision Research*, 41: 385–395.

Van Beers, R. J., Wolpert, D. M., & Haggard, P. (2001). Sensorimotor integration compensates for visual localization errors during smooth pursuit eye movements. *Journal of Neurophysioly*, 85: 1914–1922.

Vikesdal, G.H., & Langaas, T. (2016). Saccade latency and fixation stability: Repeatability and reliability. *Journal of Eye Movement Research,* 9:1-13.

Von Helmholtz, H. (1925). Treatise on Physiological Optics. *New York: Optical Society of America*, vol. 3.

Von Holst, E. (1954). Relations between the central nervous system and the peripheral organs. *British Journal of Animal Behaviour*, 2: 89–94.

Wade, N. J., Swanston, M.T. (1987). The representation of non-uniform motion: Induced movement. *Perception*, 16: 555–571.

Wallach, H., Becklen, R., & Nitzberg, D. (1985). The perception of motion during collinear eye movements. *Perception & Psychophysics*, 38: 18-22.

Wertheim, A. H. (1994). Motion perception during self-motion: the direct versus inferential controversy revisited. *Behavioral and Brain Sciences*, 17: 293–355.

Wurtz, R. H. (2008). Neuronal mechanisms of visual stability. *Vision Research*, 48 (20): 2070–2089.

Xu, Y., & Chun, M. M. (2009). Selecting and perceiving multiple visual objects. *Trends in Cognitive Sciences*, 13: 167-174.

Yantis, S. (1992). Multi-element visual tracking: attention and perceptual organization. *Cognitive Psychology*, 24: 295-340.

Yarbus, A. L. (1967). *Eye movements and vision*. New York: Plenum.

Zelinsky, G., & Todor, A. (2010). The role of "rescue saccades" in tracking objects through occlusions. *Journal of Vision*, 10(7):132.

Zhang, W., & Luck, S. J. (2008). Discrete fixed-resolution representations in visual working memory. *Nature*, 453: 233-235.

SUPPLEMENTAL INFORMATION

1. Details of the models

1.1. Fixation-Condition Models

Model F1: *Gaussian*

This model is the cumulative distribution function of a circular (wrapped) Gaussian:

$$\mathrm{CDF}(\varepsilon) = \mathrm{CDF}\{\mathrm{G}(\varepsilon; \mu, \sigma)\}, \quad (1)$$

where the cumulative distribution function $\mathrm{CDF}(\varepsilon)$ of the error variable ε (ε = reported direction of motion - actual direction of motion) is given by a Gaussian distribution $\mathrm{G}(\varepsilon; \mu, \sigma)$ whose parameters represent the accuracy (mean: μ) and the precision ($1/\sigma$, where σ is the standard deviation) of processing. The precision parameter $1/\sigma$ captures the qualitative aspect of performance, with smaller values of σ corresponding to higher qualities of encoding for the processed items.

For practical implementation, the effect of multiple wrapped Gaussians was tested in Shooner et al. (2010). Three Gaussians were initially included in the sum, and the outcome was compared with that produced by only one Gaussian. The difference was negligible due to the small variance of the distributions, which meant using a single Gaussian was sufficient to model the empirical data, and the circular nature of features could be ignored. However, we consistently applied three wraps in all conditions in the current study for the following reasons: (a) The variance of our data was large in some conditions; (b) the wrapping effect could not be ignored for the misbinding component (see Models F3c and F3r; these models were not used by Shooner et al., 2010); and (c) we observed no difference between three and five wraps.

Model F2: *Gaussian + Uniform*

In this model (Zhang & Luck, 2008), the distribution of errors is represented by:

$$\mathrm{CDF}(\varepsilon) = \mathrm{CDF}\{w.\,\mathrm{G}(\varepsilon; \mu, \sigma) + (1 - w).\,\mathrm{U}(-180,180)\}\,, \quad (2)$$

where the cumulative distribution function $\mathrm{CDF}(\varepsilon)$ is obtained from the corresponding probability density function that consists of two components:

(a) A Gaussian distribution $\mathrm{G}(\varepsilon; \mu, \sigma)$ described in the Gaussian model

(b) A uniform distribution U over the interval (-180, 180), which represents guessing

The weight of the uniform distribution (1 - w) represents the proportion of trials in which

observers base their responses on guesses rather than on the target information available. The weight *w* of the Gaussian captures the quantitative aspect of performance by providing a relative measure for the *intake* of encoding, with a larger value corresponding to a greater possibility that a response is based on having some access to information from the cued target.

Models F3c and F3r: *Gaussian + Uniform + Gaussian*

These models (Bays et al., 2009) include an additional term to account for misbinding errors when observers get confused and report another object instead of the selected target:

$$\mathrm{CDF}(\varepsilon) = \mathrm{CDF}\left\{w.\,\mathrm{G}(\varepsilon;\mu_t,\sigma_t) + (1-w-w_m).\,\mathrm{U}(-180,180) + w_m.\,\mathrm{S}^{\mathrm{T}}_{\mathrm{i=1;i\neq t}}\left[\mathrm{G}\left(\varepsilon;\mu_t+\varepsilon_{i,t},\sigma_t\right)\right]\right\}, \quad (3)$$

where the first two terms represent the same Gaussian and Uniform distributions as in the Gaussian+Uniform model and the third term represents errors stemming from misbinding reports. The selection operator $S^{T}_{i=1;i\neq t}[.]$ determines which item from the set of (*T-1*) non-cued objects is the one that generates the subject's response due to a misbinding error. An explanation for the use of this selection operator can be found in Huynh et al. (2015). Briefly, to minimize the potential interference that results from motion directions that are too close to each other, we constrained our stimuli so that no two items in any stimulus have a direction difference of less than 17 degrees. Given this constraint, we analyzed two versions of this model— i.e., misbinding with the object that is closest to the cued target in either the cued-feature space (*closest cued-feature*: Position – model F3c) or the reported-feature space (*closest reported-feature*: Motion direction – model F3r). The misbinding term is expected also to have a Gaussian distribution, with the same standard deviation as the first Gaussian but with the mean shifted from the first Gaussian by the difference $\varepsilon_{i,t}$ between the cued target's and the misbinding object's directions of motion. This is because the empirical CDF is always computed with respect to the cued target item. For the Gaussian component that describes misbinding, the wrapping effect cannot be ignored, especially when the misbinding object is shifted far away from the center of the first Gaussian. The weight w_m represents the proportion of trials in which misbinding occurs.

1.2 Smooth-Pursuit Condition Models

For all models in this section, the error variable is denoted by ε_s to emphasize the fact that we consistently computed errors in spatiotopic coordinates. On the circular ring that represents all

possible values of motion direction, the actual motion direction of the target coincides with the origin of the spatiotopic coordinate system. A conversion parameter is included where necessary to convert spatiotopic errors to equivalent retinotopic errors. The equations are similar if one prefers to compute errors in retinotopic coordinates, but the sign of the conversion parameter needs to be reversed.

Model SP1_S: *Spatiotopic Gaussian*

This model has the same form as model F1:

$$\mathrm{CDF}(\varepsilon_s) = \mathrm{CDF}\{\mathrm{G}(\varepsilon_s; \mu_s, \sigma_s)\}, \tag{4}$$

where μ_s and $1/\sigma_s$ respectively represent the accuracy and precision of spatiotopic processing.

Model SP1_R: *Retinotopic Gaussian*

This model also consists of the CDF of a circular Gaussian:

$$\mathrm{CDF}(\varepsilon_s) = \mathrm{CDF}\{\mathrm{G}(\varepsilon_s; \mu_r + \beta, \sigma_r)\}, \tag{5}$$

where μ_r and $1/\sigma_r$ respectively represent the accuracy and precision of retinotopic processing. The model assumes statistical analysis of retinotopic errors to produce a probability density function peaking near the actual retinotopic direction of motion and decaying for larger magnitudes of error. However, since the error variable ε_s is calculated with respect to the actual spatiotopic direction of motion, the mean of the Gaussian must be shifted from the origin by an angle β determined by the difference between the actual spatiotopic and retinotopic directions. This angle is given by (see Figure 4):

$$\beta = \sin^{-1}\left[\frac{|\overrightarrow{v_p}|}{|\overrightarrow{v_r}|}\sin\alpha\right], \tag{6}$$

where $|\overrightarrow{v_p}|$ and $|\overrightarrow{v_r}|$ are the magnitudes of the pursuit and retinotopic motion vectors, respectively, and α is the angle between spatiotopic and pursuit motion vectors.

Model SP1_SR: *Spatiotopic Gaussian + Retinotopic Gaussian*

This model is the CDF of a weighted sum of two circular Gaussians:

$$\mathrm{CDF}(\varepsilon_s) = \mathrm{CDF}\{w_s.\,\mathrm{G}(\varepsilon_s; \mu_s, \sigma_s) + (1 - w_s).\,\mathrm{G}(\varepsilon_s; \mu_r + \beta, \sigma_r)\}, \tag{7}$$

where the weights w_s and (1-w_s) represent the relative contributions (or *intakes*) of spatiotopic processing (with accuracy μ_s and precision $1/\sigma_s$) and retinotopic processing (with accuracy μ_r and precision $1/\sigma_r$), respectively. The means of the two components are separated by an angle β determined by equation (6). It should be noted here that, for simplicity, we have ignored the difference between μ_s and μ_r when talking about the separation between the spatiotopic and retinotopic Gaussians because they are in general very small.

Model SP2_S: *Spatiotopic Gaussian + Uniform*

This model has the same form as model F2:

$$\mathrm{CDF}(\varepsilon_s) = \mathrm{CDF}\{w_s.\,\mathrm{G}(\varepsilon_s;\mu_s,\sigma_s) + (1-w_s).\,\mathrm{U}(-180,180)\}\,, \qquad (8)$$

where the first component is the Gaussian distribution described in model SP1_S, and the second component is a uniform distribution U over the interval (-180, 180), which represents guessing. The weights w_s and (1-w_s) represent the *intake* of spatiotopic processing and guess rate, respectively.

Model SP2_R: *Retinotopic Gaussian + Uniform*

This model also has two components:

$$\mathrm{CDF}(\varepsilon_s) = \mathrm{CDF}\{w_r.\,\mathrm{G}(\varepsilon_s;\mu_r+\beta,\sigma_r) + (1-w_r).\,\mathrm{U}(-180,180)\}\,, \qquad (9)$$

where the first component is the Gaussian distribution described in model SP1_R, and the second component is a uniform distribution U over the interval (-180, 180), which represents guessing. The weights w_r and (1-w_r) represent the *intake* of retinotopic processing and guess rate, respectively. The angle β is determined by equation (6).

Model SP2_SR: *Spatiotopic Gaussian + Retinotopic Gaussian + Uniform*

This model combines models SP2_S and SP2_R and is represented by:

$$\mathrm{CDF}(\varepsilon_s) = \mathrm{CDF}\{w_s.\,\mathrm{G}(\varepsilon_s;\mu_s,\sigma_s) + w_r.\,\mathrm{G}(\varepsilon_s;\mu_r+\beta,\sigma_r) + (1-w_s-w_r).\,\mathrm{U}(-180,180)\}, \qquad (10)$$

where the weights w_s, w_r and $(1-w_s-w_r)$ represent the relative contributions (or *intakes*) of spatiotopic processing (with accuracy μ_s and precision $1/\sigma_s$), retinotopic processing (with accuracy μ_r and precision $1/\sigma_r$), and guess rate, respectively. The means of the two Gaussian distributions are separated by an angle β determined by equation (6).

Models SP3c_S and SP3r_S: *Spatiotopic Gaussian + Uniform + Spatiotopic Misbinding Gaussian*

These models are similar to models F3c and F3r but all components are assumed to be only spatiotopic:

$$\mathrm{CDF}(\varepsilon_s) = \mathrm{CDF}\{w_s.\,\mathrm{G}(\varepsilon_s;\mu_s,\sigma_s) + (1-w_s-w_{sm}).\,\mathrm{U}(-180,180) + w_{sm}.\,\mathrm{S}^{\mathrm{T}}_{\mathrm{i=1;i\neq t}}\big[\mathrm{G}\big(\varepsilon_s;\mu_s+\varepsilon_{i,t},\sigma_s\big)\big]\}, \quad (11)$$

where the first two terms represent the same Gaussian and Uniform distributions as in model SP2_S and the third term represents errors stemming from misbinding. The weights w_s, w_{sm} and $(1-w_s-w_{sm})$ represent the *intake* of spatiotopic processing (with accuracy μ_s and precision $1/\sigma_s$), misbinding rate, and guess rate, respectively. The misbinding term is expected to also have a Gaussian distribution, with the same standard deviation as the first Gaussian but with the mean shifted from the first Gaussian by the difference $\varepsilon_{i,t}$ between the cued target's and the misbinding object's directions of motion. Similar to models F3c and F3r, models SP3c_S (*closest cued feature*) and SP3r_S (*closest reported feature*) differ in how the selection operator $S^{T}_{i=1;i\neq t}[.]$ determines the misbinding item from the set of (*T-1*) non-cued objects.

Models SP3c_R and SP3r_R: *Retinotopic Gaussian + Uniform + Retinotopic Misbinding Gaussian*

These models are similar to models F3c and F3r but all components are assumed to be only retinotopic:

$$\mathrm{CDF}(\varepsilon_s) = \mathrm{CDF}\{w_r.\,\mathrm{G}(\varepsilon_s;\mu_r+\beta,\sigma_r) + (1-w_r-w_{rm}).\,\mathrm{U}(-180,180) + w_{rm}.\,\mathrm{S}^{\mathrm{T}}_{\mathrm{i=1;i\neq t}}\big[\mathrm{G}\big(\varepsilon_s;\mu_r+\varepsilon_{i,t}+\beta_i,\sigma_r\big)\big]\}, \quad (12)$$

where the first two terms represent the same Gaussian and Uniform distributions as in model SP2_R and the third term represents errors stemming from misbinding. The weights w_s, w_{rm} and $(1-w_r-w_{rm})$ represent the *intake* of retinotopic processing (with accuracy μ_r and precision $1/\sigma_r$), misbinding rate, and guess rate, respectively. The mean of the first Gaussian is shifted from the origin by an angle β determined by equation (6). Note again that μ_r (typically small) is not mentioned here for simplicity. The misbinding term is expected to also have a Gaussian distribution, with the same standard deviation as the first Gaussian but with the mean shifted from the origin by $(\varepsilon_{i,t}+\beta_i)$. In addition to the difference $\varepsilon_{i,t}$ between the cued target's and the misbinding object's spatiotopic directions of motion, the angle β_i is included to obtain the retinotopic motion direction of the misbinding item. This angle can also be computed using equation (6) but with the misbinding item's instead of the selected target's velocity vectors.

Models SP3c_SR and SP3r_SR: *Spatiotopic Gaussian + Retinotopic Gaussian + Uniform + Spatiotopic Misbinding Gaussian + Retinotopic Misbinding Gaussian*

These two models are represented by the following equation:

$$\begin{aligned}\mathrm{CDF}(\varepsilon_s) = \mathrm{CDF}\{&w_s.\,\mathrm{G}(\varepsilon_s;\mu_s,\sigma_s) + w_r.\,\mathrm{G}(\varepsilon_s;\mu_r+\beta,\sigma_r)\\ &+ (1-w_s-w_r-w_{sm}-w_{rm}).\,\mathrm{U}(-180,180)\\ &+ \mathrm{S}^{\mathrm{T}}_{\mathrm{i=1;i\neq t}}[w_{sm}.\,\mathrm{G}(\varepsilon_s;\mu_s+\varepsilon_{i,t},\sigma_s) + w_{rm}.\,\mathrm{G}(\varepsilon_s;\mu_r+\varepsilon_{i,t}+\beta_j,\sigma_t)]\}\},\end{aligned} \quad (13)$$

where the first three terms are the same spatiotopic Gaussian, retinotopic Gaussian and the Uniform distributions as in model SP2_SR, and the last two terms represent errors stemming from misbinding reports. The selection operator $S^{T}_{i=1;i\neq t}[.]$ determines from the set of (*T-1*) non-cued objects the misbinding item. Again, this can be either the '*closest cued feature'* item (model SP3c_SR) or the '*closest reported feature*' item (model SP3r_SR). Similar to the selected target, this misbinding item also produces a spatiotopic (fourth term) and a retinotopic (fifth term) Gaussian. We assume these misbinding Gaussians have the same spatiotopic and retinotopic standard deviations as the first two terms. The separations between the two spatiotopic Gaussians ($\varepsilon_{i,t}$) and between the two retinotopic Gaussians ($\varepsilon_{i,t}+\beta_j$) are determined in the same way as in models SP3c_S, SP3r_S, SP3c_R, and SP3r_R. To minimize these models' degrees of freedom, the ratio of weights for the two misbinding Gaussians is assumed to be equal to that for the two target Gaussians ($\frac{w_{sm}}{w_{rm}} = \frac{w_s}{w_r}$).

2. Bayesian inference method: Expectation-Maximization (EM) algorithm

We applied the same EM algorithm as in Huynh et al. (2015) to optimize our hypothetical models. In what follows, we modify the previous computations where necessary to reflect the consideration of reference frame as an additional factor in the models. The method, however, remains the same. It starts with a certain initial estimate for the parameters whose values will be iteratively updated by means of two alternate steps until convergence is observed.

1) The "*E step*" is to construct in the parameter space a likelihood (*L*) function that represents the probability that a given model has generated a set of data points. The expectation of *L* is then determined by evaluating its logarithm using the current estimate for the parameters.

Assume our model contains a mixture of four wrapped Gaussians and a Uniform distribution as follows [6]:

$$\mathrm{p}(\varepsilon) = w_1.\sum_{m=-\infty}^{+\infty}\mathrm{G}(\varepsilon;\mu_1 + m2\pi,\sigma_1) + w_2.\sum_{n=-\infty}^{+\infty}\mathrm{G}(\varepsilon;\mu_2 + n2\pi,\sigma_2) + w_3.\mathrm{U}(-180,180) + w_4.\sum_{p=-\infty}^{+\infty}\mathrm{G}(\varepsilon;\mu_4 + p2\pi,\sigma_4) + w_5.\sum_{q=-\infty}^{+\infty}\mathrm{G}(\varepsilon;\mu_5 + q2\pi,\sigma_5)\ , \quad (14)$$

where we have a set of thirteen parameters $\{w_1, w_2, w_3, w_4, w_5, \mu_1, \mu_2, \mu_4, \mu_5, \sigma_1, \sigma_2, \sigma_4, \sigma_5\}$ each of which has the same meaning as elaborated in the Data analyses section and in the first section of Supplementary Material, above. The first five parameters are not independent of each other but sum to one ($w_1 + w_2 + w_3, +w_4 + w_5 = 1$). Following models SP3c_SR and SP3r_SR, we further assume that $\frac{w_1}{w_2} = \frac{w_4}{w_5}$. Also, we substitute μ_s for μ_1, $(\mu_r + \beta_i)$ for μ_2 with β_i = (the angle between the cued target's spatiotopic and retinotopic motion vectors on trial *i*). Similarly, we substitute $(\mu_s + d_i)$ for μ_4, and $(\mu_r + d_i + \beta_i')$ for μ_5 with d_i = (the angle between the cued target's and the (non-cued) misbinding item's spatiotopic motion vectors on trial *i*) and β_i' = (the angle between the misbinding item's spatiotopic and retinotopic motion vectors on trial *i*). The same μ_s or μ_r appears twice in the model because subjects did not know whether they were reporting the target or a nontarget object on each trial. This also leads to the assumption that $\sigma_1 = \sigma_4 = \sigma_s$ and $\sigma_2 = \sigma_5 = \sigma_r$. The number of free parameters in the model thus reduces to seven.

Assume also that errors (ε) are produced independently across trials. From this, the likelihood function can be written as:

$$\mathrm{L} = \prod_{i=1}^{N}\mathrm{p}(\varepsilon_i)\ , \quad (15)$$

where *N* is the number of trials.

2) The "*M step*" is to find the optimal values for the parameters in the model, which are ones that maximize the *L* function.

To do that, we first take the logarithm of L:

$$\ln(\mathrm{L}) = \ln(\prod_{i=1}^{N}\mathrm{p}(\varepsilon_i)) = \sum_{i=1}^{N}\ln[\mathrm{p}(\varepsilon_i)] = \sum_{i=1}^{N}\ln[w_1.\sum_{j=-1}^{+1}\mathrm{G}_1^j + w_2.\sum_{j=-1}^{+1}\mathrm{G}_2^j + w_3.\mathrm{U} + w_4.\sum_{j=-1}^{+1}\mathrm{G}_4^j + w_5.\sum_{j=-1}^{+1}\mathrm{G}_5^j]\ , \quad (16)$$

[6] The model of this form can be considered as a generalization for all of our hypothetical models (see models SP3c_SR and SP3r_SR in the Smooth-Pursuit Condition Models section). Note that, for simplification, we did not include the summation operators to represent wrapped Gaussians in those models.

where:

$$G_1^j = \frac{1}{\sigma_S\sqrt{2\pi}} e^{-\frac{(\varepsilon_i-\mu_S-j2\pi)^2}{2\sigma_S^2}} \qquad G_2^j = \frac{1}{\sigma_r\sqrt{2\pi}} e^{-\frac{(\varepsilon_i-\mu_r-\beta_i-j2\pi)^2}{2\sigma_r^2}}$$

$$G_4^j = \frac{1}{\sigma_S\sqrt{2\pi}} e^{-\frac{(\varepsilon_i-\mu_S-d_i-j2\pi)^2}{2\sigma_S^2}} \qquad G_5^j = \frac{1}{\sigma_r\sqrt{2\pi}} e^{-\frac{(\varepsilon_i-\mu_r-d_i-\beta_i'-j2\pi)^2}{2\sigma_r^2}}$$

(with j = -1, 0, 1). For simplicity, we have dropped in Equation 16 the arguments of the Gaussian and uniform distributions, reduced the number of Gaussians of each component to three (for the reasons provided under Data analysis and in the first section of Supplementary Material, above), and used the subscripts of the Gaussians to distinguish the different components of the model.

The function $\ln(L)$ is then evaluated by using *Jensen's inequality* [7]:

$$\ln(L) \geq$$

$$\sum_{i=1}^{N}\{ \sum_{j=-1}^{+1} p^0\left(G_1^j|\varepsilon_i\right).\ln\left(\frac{w_1.G_1^j}{p^0\left(G_1^j|\varepsilon_i\right)}\right) + \sum_{j=-1}^{+1} p^0\left(G_2^j|\varepsilon_i\right).\ln\left(\frac{w_2.G_2^j}{p^0\left(G_2^j|\varepsilon_i\right)}\right) + p^0(U|\varepsilon_i).\ln\left(\frac{w_3.U}{p^0(U|\varepsilon_i)}\right) +$$

$$+ \sum_{j=-1}^{+1} p^0\left(G_4^j|\varepsilon_i\right).\ln\left(\frac{w_4.G_4^j}{p^0\left(G_4^j|\varepsilon_i\right)}\right) + \sum_{j=-1}^{+1} p^0\left(G_5^j|\varepsilon_i\right).\ln\left(\frac{w_5.G_5^j}{p^0\left(G_5^j|\varepsilon_i\right)}\right)\}, \qquad (17)$$

where $p^0\left(G_1^j|\varepsilon_i\right)$, $p^0\left(G_2^j|\varepsilon_i\right)$, $p^0(U|\varepsilon_i)$, $p^0\left(G_4^j|\varepsilon_i\right)$, $p^0\left(G_5^j|\varepsilon_i\right)$ represent the probabilities that a data point is most likely to be captured by the first Gaussian, the second Gaussian, the Uniform, the third Gaussian, and the fourth Gaussian distributions in the model, respectively, given its value ε_i. Note that the superscript *'0'* indicates the "*current*" status of the parameters, which has sneaked in the inequality in the form of conditional probability. From Bayes' theorem, we have:

$$p^0\left(G_1^j|\varepsilon_i\right) = \frac{w_1^0.G\left(\varepsilon_i;\mu_S^0+j2\pi,\sigma_S^0\right)}{p^0(\varepsilon_i)} \qquad p^0\left(G_2^j|\varepsilon_i\right) = \frac{w_1^0.G\left(\varepsilon_i;\mu_r^0+\beta_i+j2\pi,\sigma_r^0\right)}{p^0(\varepsilon_i)}$$

$$p^0(U|\varepsilon_i) = \frac{w_3^0.U}{p^0(\varepsilon_i)}$$

$$p^0\left(G_4^j|\varepsilon_i\right) = \frac{w_1^0.G\left(\varepsilon_i;\mu_S^0+d_i+j2\pi,\sigma_S^0\right)}{p^0(\varepsilon_i)} \qquad p^0\left(G_5^j|\varepsilon_i\right) = \frac{w_1^0.G\left(\varepsilon_i;\mu_r^0+d_i+\beta_i'+j2\pi,\sigma_r^0\right)}{p^0(\varepsilon_i)}$$

The right hand side of (Eq.17) is the lower bound of $\ln(L)$, so we want to maximize its value. The inequality can be rewritten as:

$$\ln(L) \geq$$

$$\sum_{i=0}^{n}\{ \sum_{j=-1}^{+1} p^0\left(G_1^j|\varepsilon_i\right).\ln(w_1.G_1^j) + \sum_{j=-1}^{+1} p^0\left(G_2^j|\varepsilon_i\right).\ln(w_2.G_2^j) + p^0(U|\varepsilon_i).\ln(w_3.U) +$$

[7] Jensen's inequality: $\ln(\sum_{j=1}^{T} c_j) = \ln(\sum_{j=1}^{T} \frac{c_j}{p_j}.p_j) \geq \sum_{j=1}^{T} p_j.\ln(\frac{c_j}{p_j})$

$$\sum_{j=-1}^{+1} \mathrm{p}^0\left(\mathrm{G}_4^j|\varepsilon_i\right).\ln(w_4.\mathrm{G}_1^j) + \sum_{j=-1}^{+1} \mathrm{p}^0\left(\mathrm{G}_5^j|\varepsilon_i\right).\ln(w_5.\mathrm{G}_5^j)\ \} -$$
$$\sum_{i=0}^{n}\{\ \sum_{j=-1}^{+1} \mathrm{p}^0\left(\mathrm{G}_1^j|\varepsilon_i\right).\ln(\mathrm{p}^0\left(\mathrm{G}_1^j|\varepsilon_i\right)) + \sum_{j=-1}^{+1} \mathrm{p}^0\left(\mathrm{G}_2^j|\varepsilon_i\right).\ln(\mathrm{p}^0\left(\mathrm{G}_2^j|\varepsilon_i\right)) +$$
$$\mathrm{p}^0(\mathrm{U}|\varepsilon_i).\ln(\mathrm{p}^0(\mathrm{U}|\varepsilon_i)) + \sum_{j=-1}^{+1} \mathrm{p}^0\left(\mathrm{G}_4^j|\varepsilon_i\right).\ln(\mathrm{p}^0\left(\mathrm{G}_4^j|\varepsilon_i\right)) + \sum_{j=-1}^{+1} \mathrm{p}^0\left(\mathrm{G}_5^j|\varepsilon_i\right).\ln(\mathrm{p}^0\left(\mathrm{G}_5^j|\varepsilon_i\right))\ \},$$
(18)

Because the second summation is a constant, the problem boils down to finding the new values for the parameters that maximize the first summation (*S*):

$$S = \sum_{i=0}^{n}\{\ \sum_{j=-1}^{+1} \mathrm{p}^0\left(\mathrm{G}_1^j|\varepsilon_i\right).\ln(w_1.\mathrm{G}_1^j) + \sum_{j=-1}^{+1} \mathrm{p}^0\left(\mathrm{G}_2^j|\varepsilon_i\right).\ln(w_2.\mathrm{G}_2^j) + \mathrm{p}^0(\mathrm{U}|\varepsilon_i).\ln(w_3.\mathrm{U}) +$$
$$\sum_{j=-1}^{+1} \mathrm{p}^0\left(\mathrm{G}_4^j|\varepsilon_i\right).\ln(w_4.\mathrm{G}_1^j) + \sum_{j=-1}^{+1} \mathrm{p}^0\left(\mathrm{G}_5^j|\varepsilon_i\right).\ln(w_5.\mathrm{G}_5^j)\ \},$$
(19)

We do so by taking partial derivatives of *S* with respect to each parameter, setting each derivative equal to zero, and solving the equations[8]. The results are (note that the superscript '*1*' indicates the "*updated*" values for the parameters):

$$\mu_s^1 = \sum_{i=1}^{N}\{\ \varepsilon_i.\left(\sum_{j=-1}^{+1} \mathrm{p}^0\left(\mathrm{G}_1^j|\varepsilon_i\right) + \sum_{j=-1}^{+1} \mathrm{p}^0\left(\mathrm{G}_4^j|\varepsilon_i\right)\right) + 2\pi.\left(\mathrm{p}^0(\mathrm{G}_1^{-1}|\varepsilon_i) - \mathrm{p}^0(\mathrm{G}_1^1|\varepsilon_i) +$$
$$\mathrm{p}^0(\mathrm{G}_4^{-1}|\varepsilon_i) - \mathrm{p}^0(\mathrm{G}_4^1|\varepsilon_i)\right) - d_i.\sum_{j=-1}^{+1} \mathrm{p}^0\left(\mathrm{G}_4^j|\varepsilon_i\right)\} \div \sum_{i=1}^{N}\{\sum_{j=-1}^{+1} \mathrm{p}^0\left(\mathrm{G}_1^j|\varepsilon_i\right) + \sum_{j=-1}^{+1} \mathrm{p}^0\left(\mathrm{G}_4^j|\varepsilon_i\right)\}$$
$$\mu_r^1 = \sum_{i=1}^{N}\{\ \varepsilon_i.\left(\sum_{j=-1}^{+1} \mathrm{p}^0\left(\mathrm{G}_2^j|\varepsilon_i\right) + \sum_{j=-1}^{+1} \mathrm{p}^0\left(\mathrm{G}_5^j|\varepsilon_i\right)\right) + 2\pi.\left(\mathrm{p}^0(\mathrm{G}_2^{-1}|\varepsilon_i) - \mathrm{p}^0(\mathrm{G}_2^1|\varepsilon_i) +$$
$$\mathrm{p}^0(\mathrm{G}_5^{-1}|\varepsilon_i) - \mathrm{p}^0(\mathrm{G}_5^1|\varepsilon_i)\right) - \beta_i.\sum_{j=-1}^{+1} \mathrm{p}^0\left(\mathrm{G}_2^j|\varepsilon_i\right) - (d_i + \beta_i').\sum_{j=-1}^{+1} \mathrm{p}^0\left(\mathrm{G}_5^j|\varepsilon_i\right)\} \div$$
$$\sum_{i=1}^{N}\{\sum_{j=-1}^{+1} \mathrm{p}^0\left(\mathrm{G}_2^j|\varepsilon_i\right) + \sum_{j=-1}^{+1} \mathrm{p}^0\left(\mathrm{G}_5^j|\varepsilon_i\right)\}$$
$$\sigma_s^1 = \left[\sum_{i=1}^{N}\{\sum_{j=-1}^{+1} \mathrm{p}^0\left(\mathrm{G}_1^j|\varepsilon_i\right).(\varepsilon_i - \mu_s^1 - j2\pi)^2 + \sum_{j=-1}^{+1} \mathrm{p}^0\left(\mathrm{G}_4^j|\varepsilon_i\right).(\varepsilon_i - \mu_s^1 - d_i - j2\pi)^2\}\right]^{1/2} \div$$
$$\left[\sum_{i=1}^{N}\{\sum_{j=-1}^{+1} \mathrm{p}^0\left(\mathrm{G}_1^j|\varepsilon_i\right) + \sum_{j=-1}^{+1} \mathrm{p}^0\left(\mathrm{G}_4^j|\varepsilon_i\right)\}\right]^{1/2}$$
$$\sigma_r^1 = \left[\sum_{i=1}^{N}\{\sum_{j=-1}^{+1} \mathrm{p}^0\left(\mathrm{G}_2^j|\varepsilon_i\right).(\varepsilon_i - \mu_s^1 - \beta_i - j2\pi)^2 + \sum_{j=-1}^{+1} \mathrm{p}^0\left(\mathrm{G}_5^j|\varepsilon_i\right).(\varepsilon_i - \mu_s^1 - d_i - \beta_i' -\right.$$
$$\left.j2\pi)^2\}\right]^{1/2} \div \left[\sum_{i=1}^{N}\{\sum_{j=-1}^{+1} \mathrm{p}^0\left(\mathrm{G}_2^j|\varepsilon_i\right) + \sum_{j=-1}^{+1} \mathrm{p}^0\left(\mathrm{G}_5^j|\varepsilon_i\right)\}\right]^{1/2}$$
$$w_1^1 = w_s^1 = \frac{1}{N}\sum_{i=1}^{N}\sum_{j=-1}^{+1} \mathrm{p}^0\left(\mathrm{G}_1^j|\varepsilon_i\right) \qquad w_2^1 = w_r^1 = \frac{1}{N}\sum_{i=1}^{N}\sum_{j=-1}^{+1} \mathrm{p}^0\left(\mathrm{G}_2^j|\varepsilon_i\right)$$
$$w_3^1 = w_{\mathrm{U}}^1 = \frac{1}{N}\sum_{i=1}^{N} p^0(\mathrm{U}|\varepsilon_i)$$
$$w_4^1 = \frac{w_1^1}{w_1^1 + w_2^1}.(1 - w_1^1 - w_2^1 - w_3^1) \qquad w_5^1 = \frac{w_2^1}{w_1^1 + w_2^1}.(1 - w_1^1 - w_2^1 - w_3^1)$$

with $p^o(G_1|\varepsilon_i), p^o(G_2|\varepsilon_i),$ and $p^o(U|\varepsilon_i)$ given by equations (Eq.11), (Eq.12), and (Eq.13). These "*updated*" values become the "*current*" values in the next iteration and the algorithm iterates these

[8] Here, the second order derivatives are found to be negative in all cases.

computations for the parameters until convergence to a certain local maximum of the likelihood function.

3. Bayesian-model comparison

We used penalized likelihood criteria of the Akaike information criterion (AIC) and Bayesian information criterion (BIC) for model selection. The AIC and BIC for a model are defined as:

$$AIC = -2\ln(L) + 2p\,, \tag{20}$$

$$BIC = -2\ln(L) + pln(n), \tag{21}$$

where L represents the maximized value of the likelihood function of the model (obtained from the EM algorithm), p is the number of free parameters in the model, and n is sample size. These two criteria try to balance a good fit with the parsimony of a model. Given a set of models, the selected model is the one with minimum AIC or BIC values. If two models yield AIC or BIC values that are insignificantly different from each other, the model with fewer parameters is preferred according to Occam's razor.

4. Bayesian results

Model selection

Comparisons of *AIC* values result in the same winning models as in the Least Squares method. In the fixation condition, the three models F2, F3c, and F3r have equivalent performance, which is significantly better than that of model F1. In the SPEM condition, performance is equivalent for the SP2_*, SP3c_*, and SP3r_* groups, which is significantly better than the SP1 group. Equivalent performance was also found for the spatiotopic (*_S) and combined (*_SR) groups, which is significantly better than that of the retinotopic (*_R) group. Comparisons of *BIC* values additionally show that model F2 performs significantly better than models F3c and F3r, and the SP2_* group performs significantly better than the groups SP3c_* and SP3r_*. Combined, the models F2 and SP2_S are selected, the same as when using the Least Squares method.

Parameter estimation

Estimates of *intake* and *precision* parameters by Bayesian analysis are shown in figures S1 (experiments 1a and 2a) and S2 (experiments 1b and 2b).

----- insert Figures S1 and S2 here -----

5. Actual vs theoretical eye movements

The pursuit system is not perfect in that the eye is in general not perfectly aligned with the pursuit target and may be slightly lagging behind or running ahead. To ensure accuracy and to take into account the actual *proximal* stimulus, our approach for the decomposition of spatiotopic and retinotopic components shown in Figure 4 was therefore performed based on the *actual* eye-velocity vector instead of that of the pursuit target. However, to ensure that the noise introduced by the pursuit system did not fundamentally influence our analyses and conclusions, we have also carried out the decomposition based on theoretical eye movements (i.e., the velocity of the pursuit target). Figure S3 shows a comparison of results for individual observers computed by using the actual (upper panels; data replotted from Fig. 9) and the theoretical eye movements (lower panels). The inspection of the figure shows that the results are similar and the same trend is observed for the data averaged across the observers (Table S1).

----- insert Figure S3 here -----

----- insert Table S1 here -----

Figure and Table Legends

Figure 1. Time course of a trial in the fixation condition: Experiments 1a (varying set size; no cue delay) and 1b (set size fixed; varying cue delay).

Figure 2. Illustration of the step-ramp paradigm: changes of the pursuit target and eye position along the pursuit direction as a function of time.

Figure 3. Time course of a trial in the smooth pursuit eye movement (SPEM) condition: Experiments 2a (varying set size; no cue delay) and 2b (set size fixed; varying cue delay). The gray central dot, dashed circle, and dashed arrows are shown for illustration purposes only; they are invisible during the experiments.

Figure 4. Decomposition of spatiotopic and retinotopic motion vectors: $\overrightarrow{v_s}$, $\overrightarrow{v_r}$, and $\overrightarrow{v_p}$ represent the velocity of the target object with respect to the screen (spatiotopic vector), velocity of the target object with respect to the projected fovea (retinotopic vector), and pursuit (eye) velocity, respectively. Spatiotopic error is measured as the angular deviation between the reported and the spatiotopic vectors. Retinotopic error is measured as the angular deviation between the reported and the retinotopic vectors.

Figure 5. Two-dimensional gaze traces on example SPEM trials (observer TAN, Experiment 2a) shown in different colors within the 10x10-deg central area of the screen. The 3-deg, 4-deg, and 1-deg gray circles represent the initial fixation, jump-back, and terminal positions of the pursuit target, respectively. The central cross marks the center of the screen.

Figure 6. Eye position (*colored lines;* 7 trials in Experiment 2a, observer TAN) shown with the pursuit target's position (*black solid line*) along the pursuit direction as a function of time. The 0-deg position represents the center of the display. The shaded area represents the critical time window within which pursuit gain must fall in the specified range, and no saccades and blinks are allowed (See also figure 2).

Figure 7. Eye velocity data for an example SPEM trial (observer TAN, Experiment 2a): raw velocity (green) and low-pass filtered (blue) data. The black line represents the average of filtered traces obtained from 100 randomly selected trials (observer TAN, Experiment 2a). The shaded area shows the constrained range for averaged velocity in the critical pursuit interval.

Figure 8. Data for individual observers in Experiments 1a (fixation; left panel) and 2a (SPEM; right panel): Transformed performance (left y-axes) and error magnitude (right y-axes) plotted as a function of set size. SPEM performance in the right panel was measured in *spatiotopic* coordinates. Error bars correspond to ±1 standard error of the mean.

Figure 9. Data for individual observers in Experiment 2a (SPEM). Left panel: SPEM transformed performance (left y-axes) and error magnitude (right y-axes) measured in *retinotopic* coordinates as a function of set size. Right panel: same as left panel expressed with respect to spatiotopic performance, under the assumption that spatiotopic performance is perfect (zero spatiotopic errors). Error bars correspond to ±1 standard error of the mean.

Figure 10. Average data in Experiments 1a (fixation) and 2a (SPEM): Transformed performance (left y-axis) and error magnitude (right y-axis) averaged across observers as a function of set size for 3 cases: *Fixation* (red), *SPEM spatiotopic* (green), *SPEM retinotopic* (blue). Error bars correspond to ±1 standard error of the mean.

Figure 11. Data for individual observers in Experiments 1b (fixation; left panel) and 2b (SPEM; center and right panels): Transformed performance (left y-axes) and error magnitude (right y-axes) plotted as a function of cue-delay. Performance during SPEM in the center and right panels was measured in *spatiotopic* and *retinotopic* coordinates, respectively. Error bars correspond to ±1 standard error of the mean.

Figure 12. Average data in Experiments 1b (fixation) and 2b (SPEM): Transformed performance (left y-axis) and error magnitude (right y-axis) averaged across observers as a function of cue delay for 3 cases: *Fixation* (red), *SPEM spatiotopic* (green), *SPEM retinotopic* (blue). Error bars correspond to ±1 standard error of the mean.

Figure 13. Decomposition of performance in Experiments 1a (fixation; left column) and 2a (SPEM; right column): Intake along with guess rate (upper row) and precision (lower row), averaged across observers, are shown as a function of set size. Data are shown for only the winning model in each condition (see top of each panel). Error bars correspond to ±1 standard error of the mean.

Figure 14. Decomposition of performance in Experiments 1b (fixation; left column) and 2b (SPEM; right column): Intake (upper row) and precision (lower row), averaged across observers, are shown as a function of cue delay. Data are shown for only the winning model in each condition (see top of each panel). Error bars correspond to ±1 standard error of the mean. Data for a set size of 1, shown

only at cue delay = 0 s, are taken from Experiment 1. Horizontal lines are to indicate that performance in this condition is largely independent of cue delay.

Figure S1. Same as Figure 13 but with data obtained from Bayesian Analysis.

Figure S2. Same as Figure 14 but with data obtained from Bayesian Analysis.

Figure S3. Comparison of results obtained by using the actual eye movement (upper panels; replot of Figure 9) with those obtained by using the theoretical eye movement (i.e., by using the pursuit target velocity) for individual observer data. Overall, similar results are obtained, as is the case for the data averaged across the observers (Table S1).

Table 1. Mean adjusted-R^2 values, obtained from the Least-Squares fitting method, for different models and conditions.

Table S1. Comparison of results obtained by using the actual eye movement (Fig. 10, blue line) with those obtained by using the theoretical eye movement for data averaged across observers.

Supplementary Material

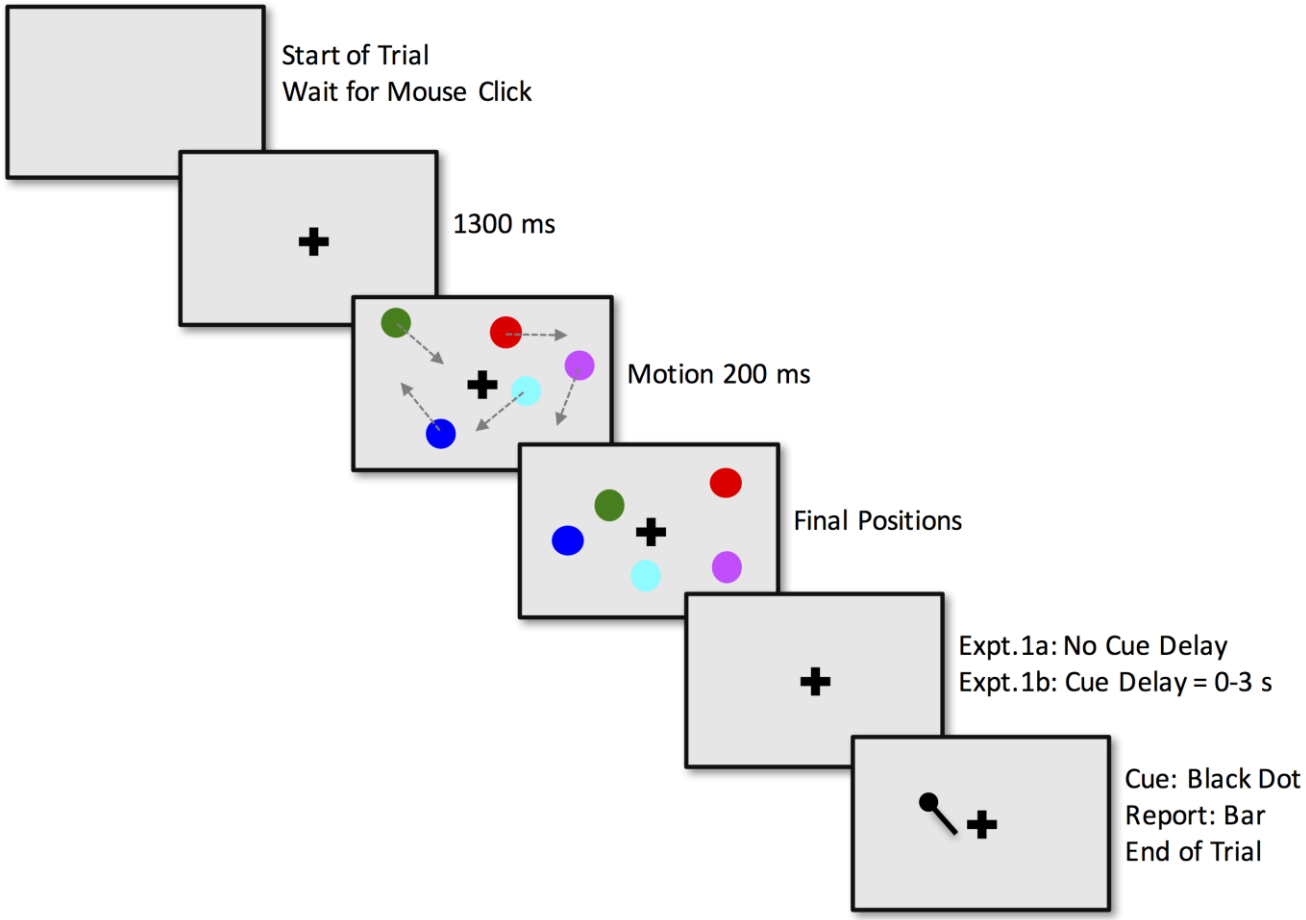
Start of Trial
Wait for Mouse Click
1300 ms
Motion 200 ms
Final Positions
Expt.1a: No Cue Delay
Expt.1b: Cue Delay = 0-3 s
Cue: Black Dot
Report: Bar
End of Trial

Figure 1

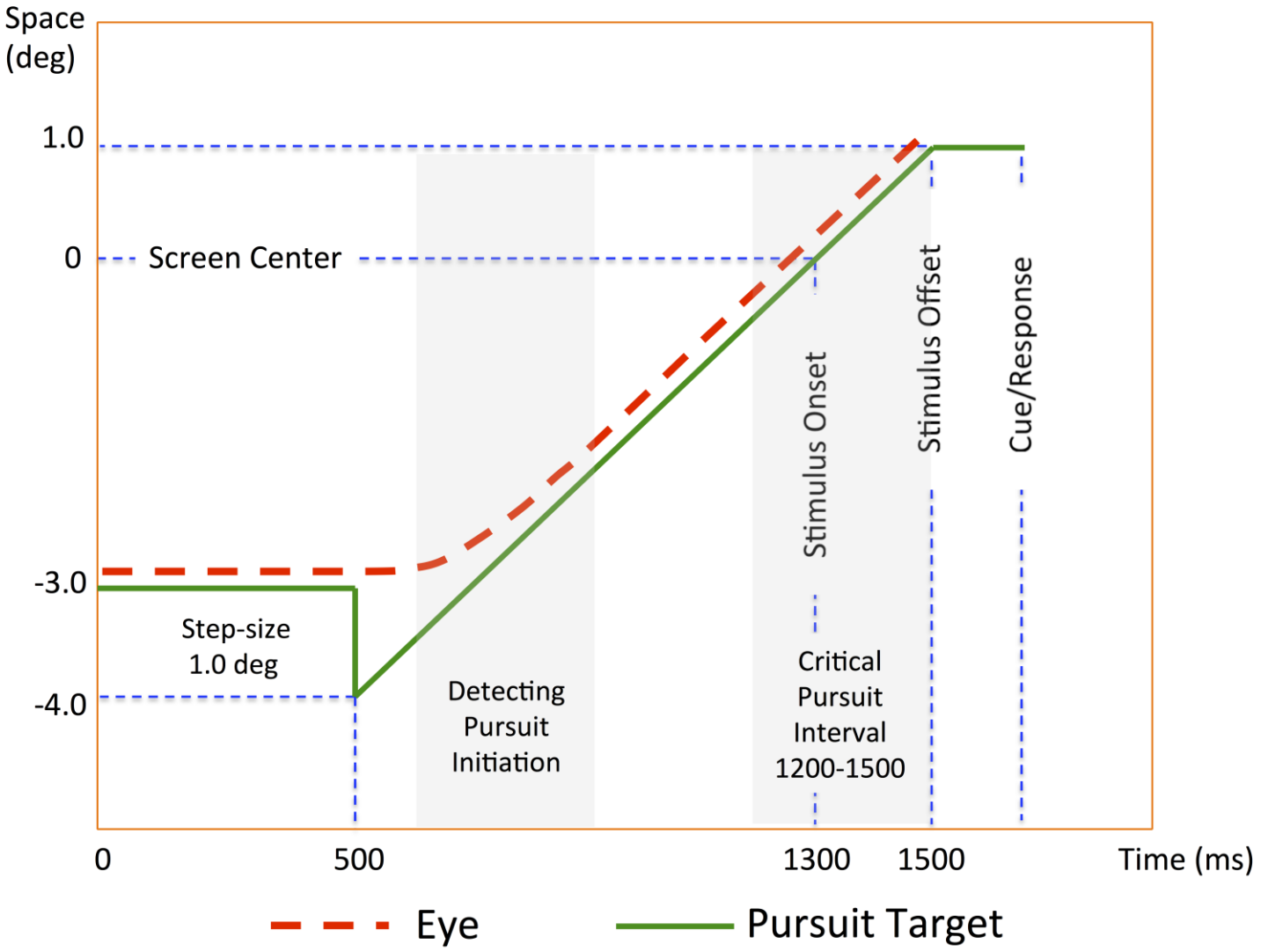
Space
(deg)
1.0
0
Screen Center
-3.0
-4.0
Step-size
1.0 deg
Detecting
Pursuit
Initiation
Stimulus Onset
Critical
Pursuit
Interval
1200-1500
Stimulus Offset
Cue/Response
0
500
1300
1500
Time (ms)
Eye
Pursuit Target

Figure 2

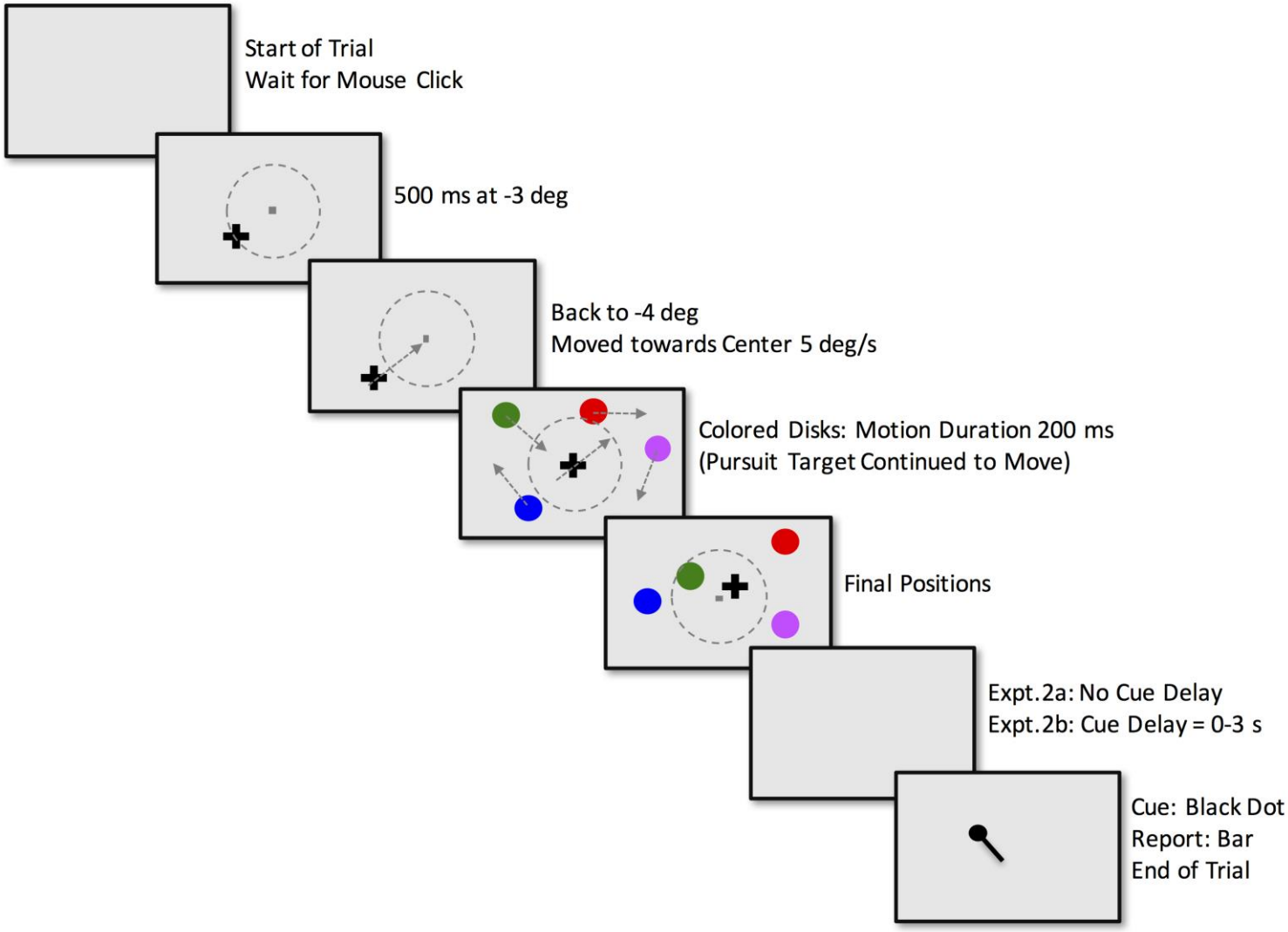
Start of Trial
Wait for Mouse Click
500 ms at -3 deg
Back to -4 deg
Moved towards Center 5 deg/s
Colored Disks: Motion Duration 200 ms
(Pursuit Target Continued to Move)
Final Positions
Expt.2a: No Cue Delay
Expt.2b: Cue Delay = 0-3 s
Cue: Black Dot
Report: Bar
End of Trial

Figure 3

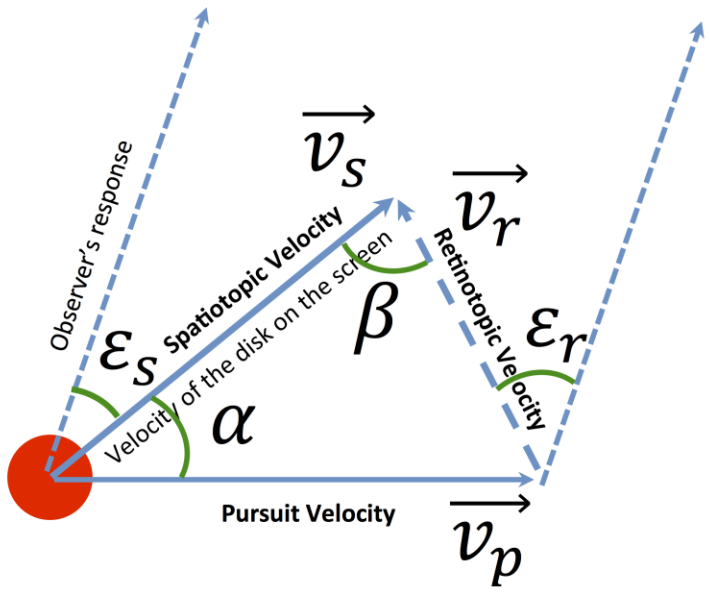

ε_s spatiotopic error

ε_r retinotopic error
(converted to spatiotopic error in model equations)

$$\overrightarrow{v_s} = \overrightarrow{v_r} + \overrightarrow{v_p}$$

Figure 4

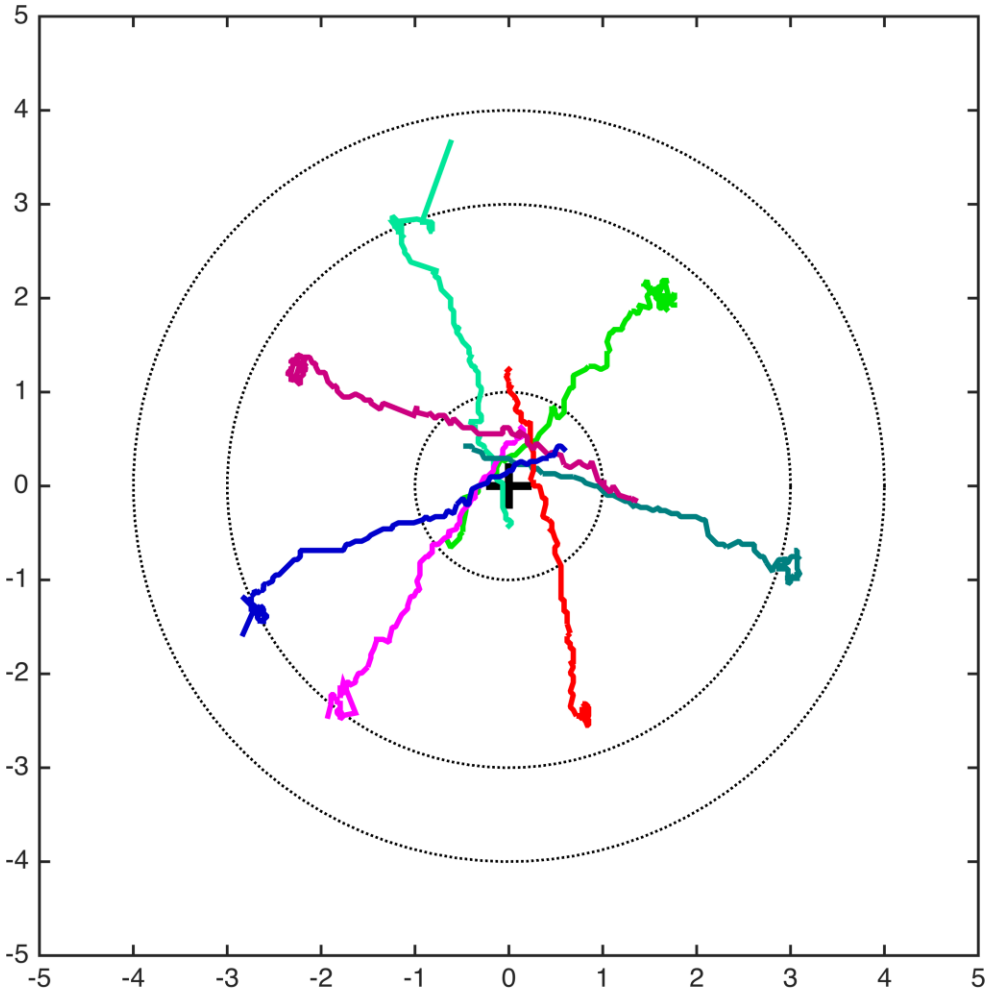

Figure 5

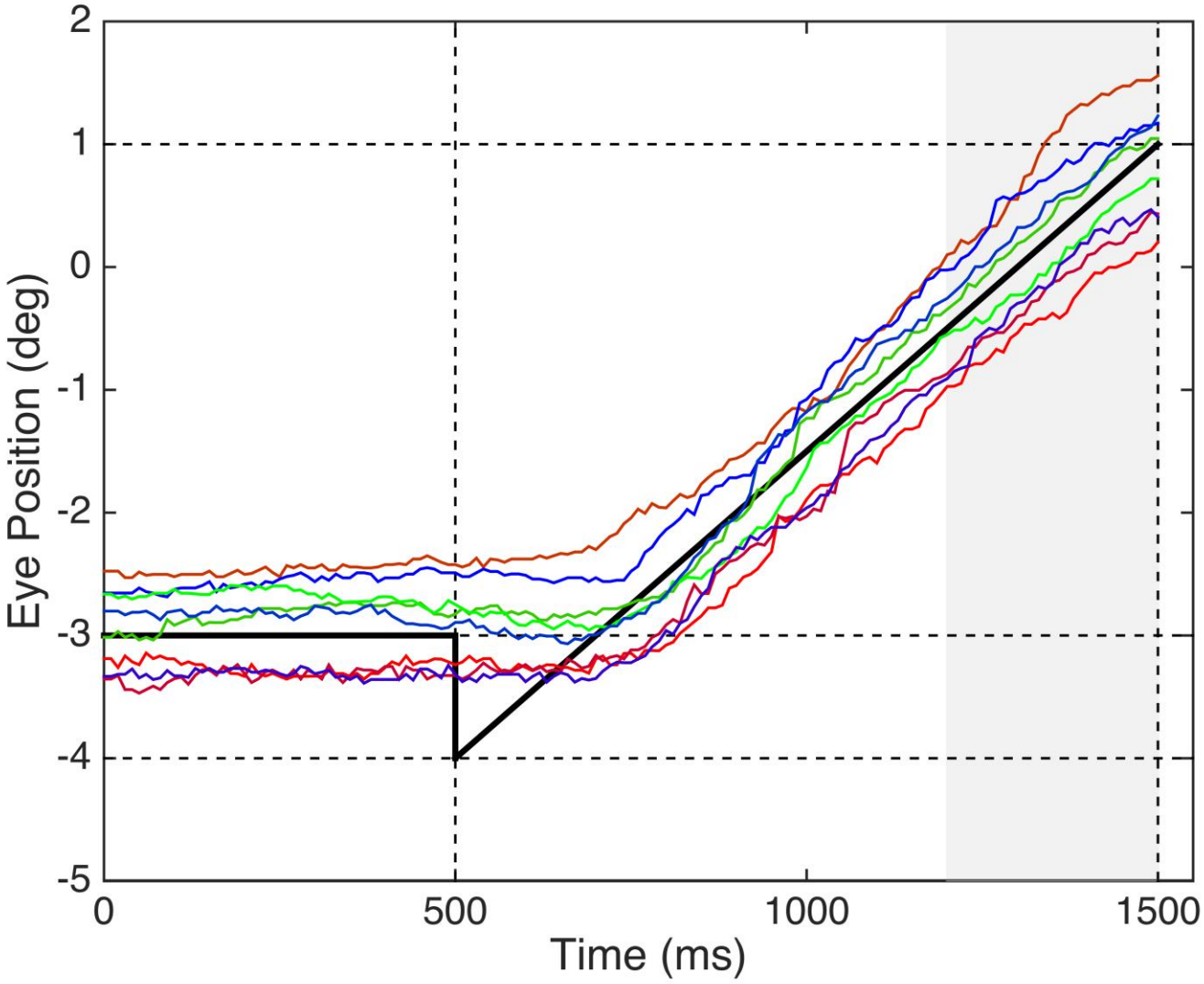

Figure 6

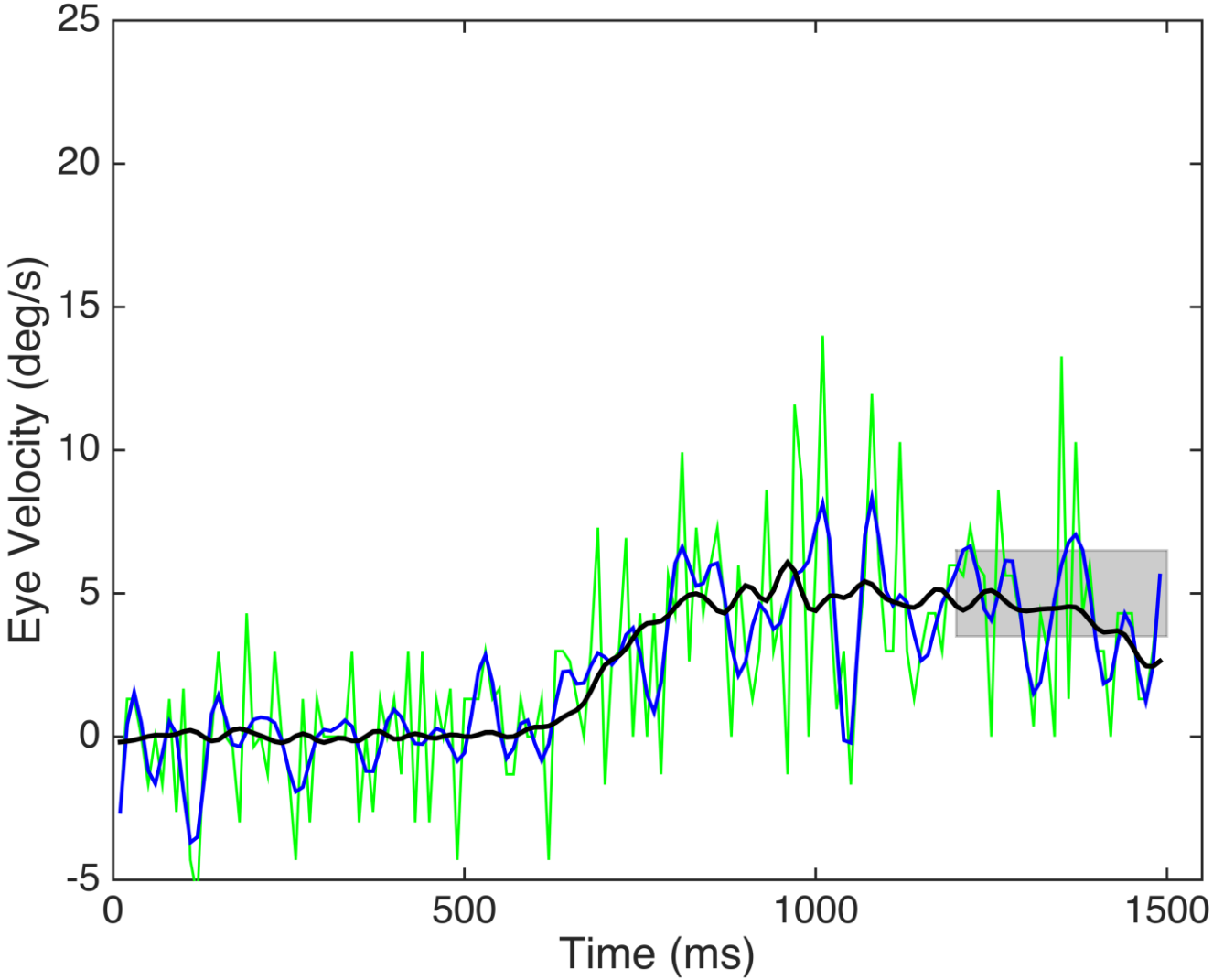

Figure 7

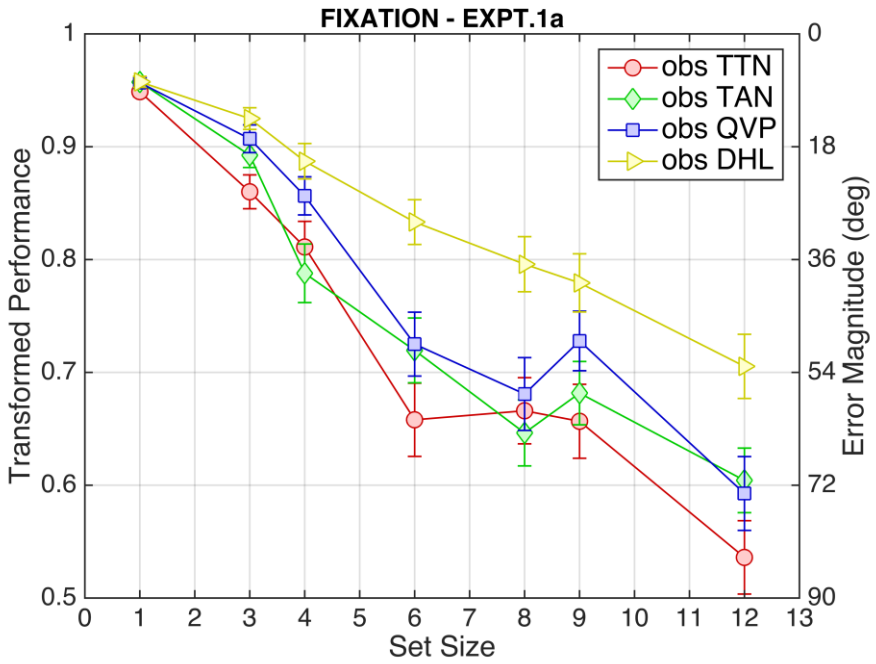
FIXATION - EXPT.1a
obs TTN
obs TAN
obs QVP
obs DHL
Transformed Performance
Error Magnitude (deg)
Set Size
1
0.9
0.8
0.7
0.6
0.5
0
18
36
54
72
90
0 1 2 3 4 5 6 7 8 9 10 11 12 13

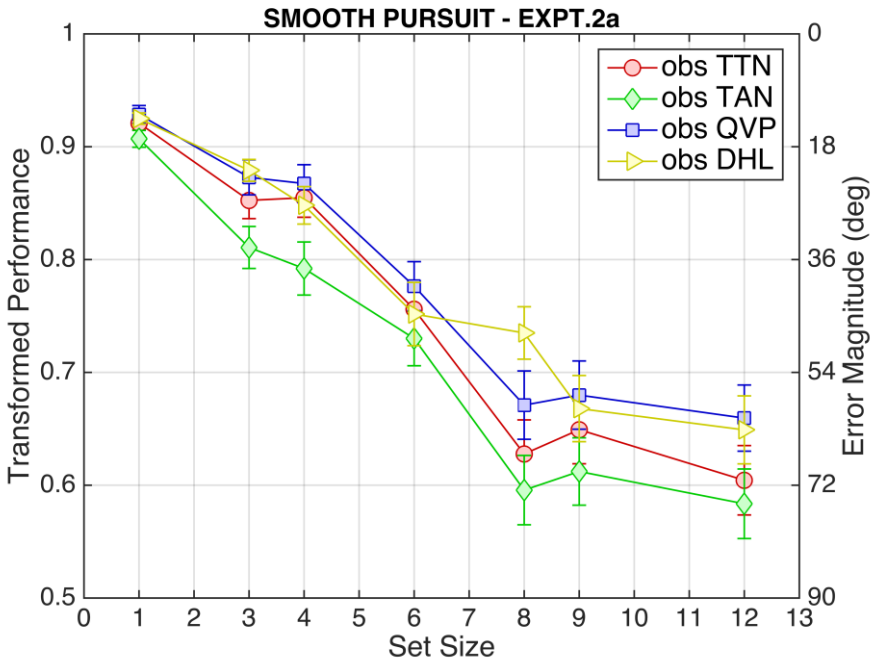
SMOOTH PURSUIT - EXPT.2a
obs TTN
obs TAN
obs QVP
obs DHL
Transformed Performance
Error Magnitude (deg)
Set Size
1
0.9
0.8
0.7
0.6
0.5
0
18
36
54
72
90
0 1 2 3 4 5 6 7 8 9 10 11 12 13

Figure 8

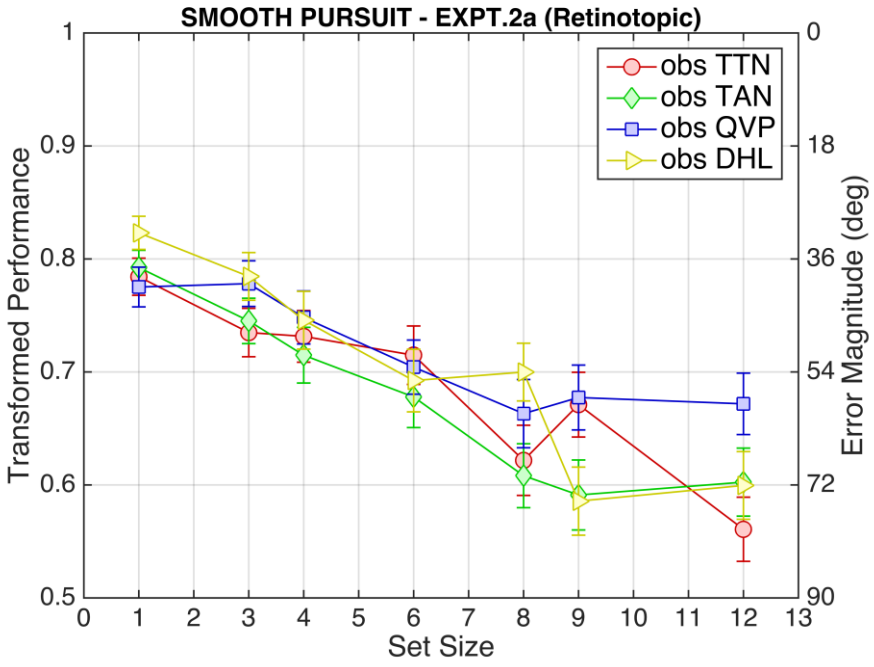
SMOOTH PURSUIT - EXPT.2a (Retinotopic)
obs TTN
obs TAN
obs QVP
obs DHL
Transformed Performance
Error Magnitude (deg)
Set Size
1
0.9
0.8
0.7
0.6
0.5
0
18
36
54
72
90
0 1 2 3 4 5 6 7 8 9 10 11 12 13

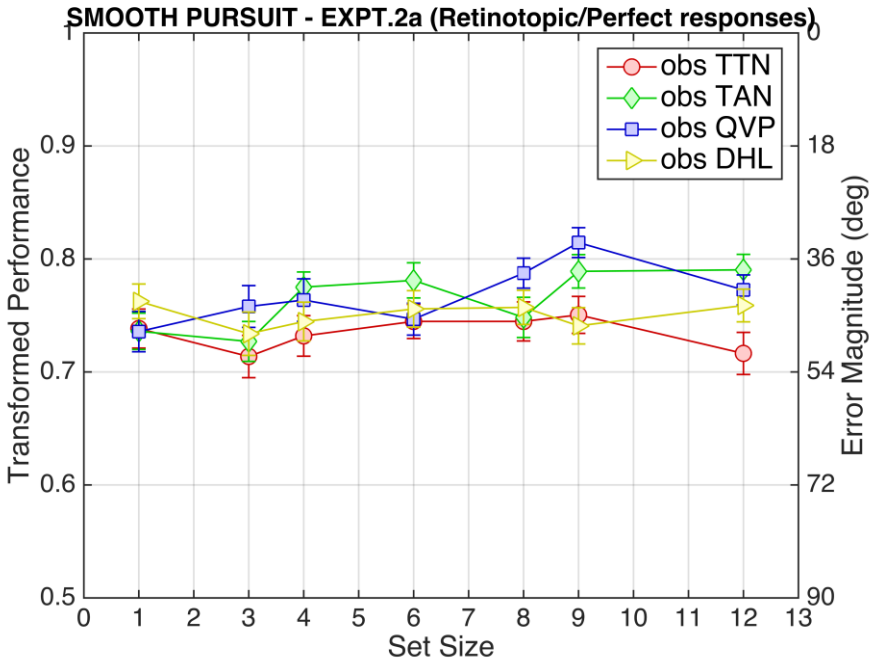
SMOOTH PURSUIT - EXPT.2a (Retinotopic/Perfect responses)
obs TTN
obs TAN
obs QVP
obs DHL
Transformed Performance
Error Magnitude (deg)
Set Size
1
0.9
0.8
0.7
0.6
0.5
0
18
36
54
72
90
0 1 2 3 4 5 6 7 8 9 10 11 12 13

Figure 9

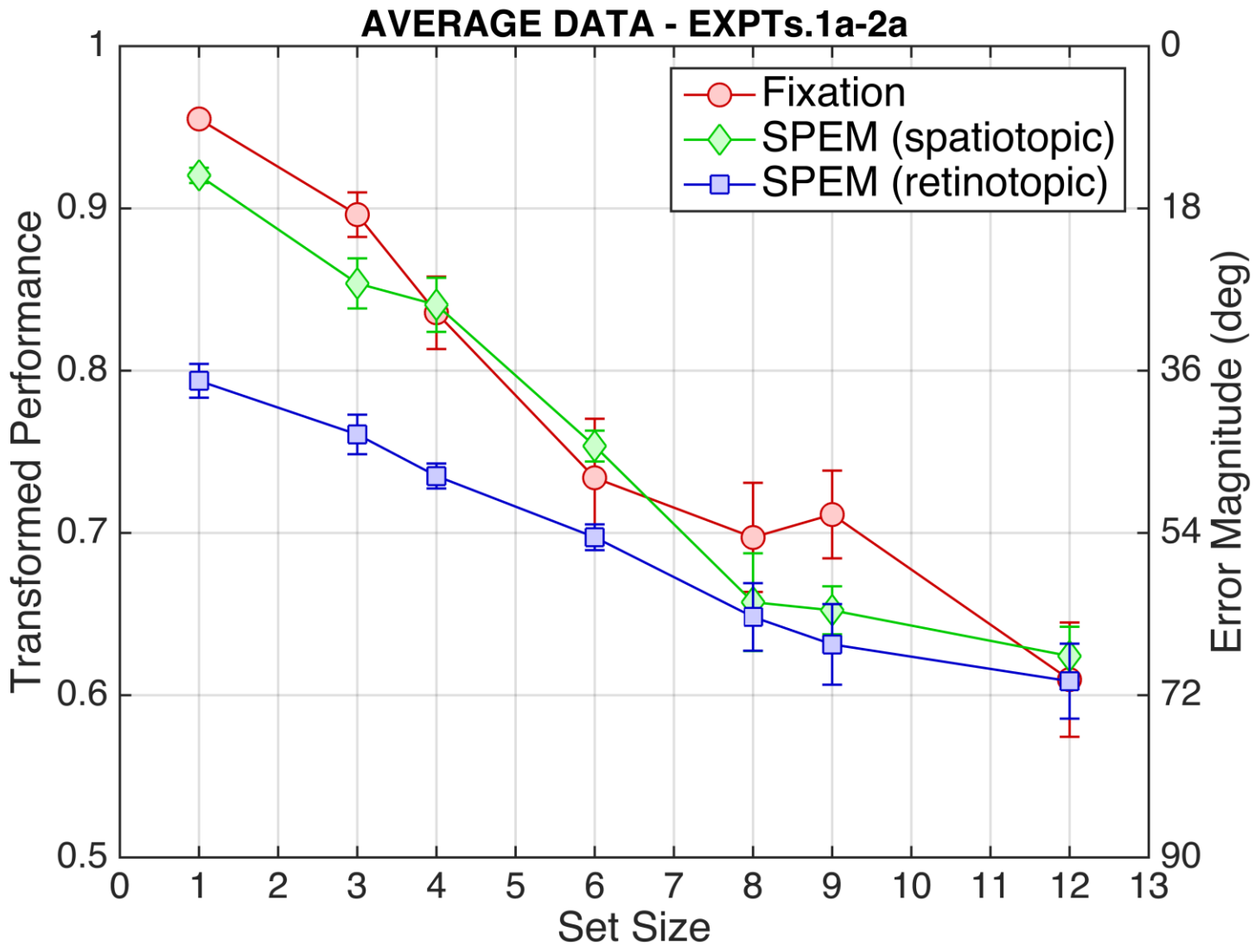
AVERAGE DATA - EXPTs.1a-2a
Fixation
SPEM (spatiotopic)
SPEM (retinotopic)
Transformed Performance
Error Magnitude (deg)
Set Size
1
0.9
0.8
0.7
0.6
0.5
0
18
36
54
72
90
0
1
2
3
4
5
6
7
8
9
10
11
12
13

Figure 10

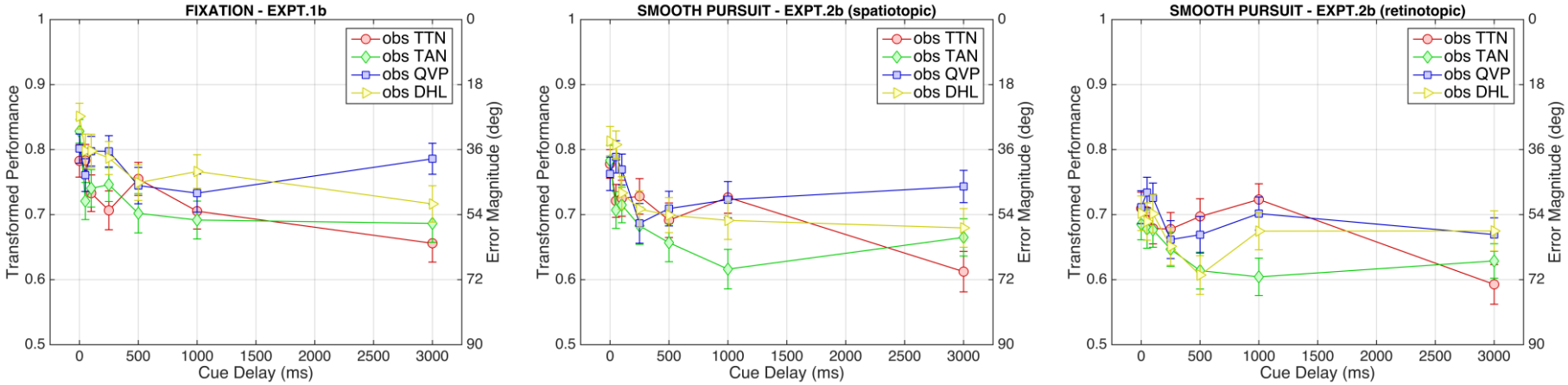
FIXATION - EXPT.1b
SMOOTH PURSUIT - EXPT.2b (spatiotopic)
SMOOTH PURSUIT - EXPT.2b (retinotopic)
obs TTN
obs TAN
obs QVP
obs DHL
Transformed Performance
Error Magnitude (deg)
Cue Delay (ms)
1
0.9
0.8
0.7
0.6
0.5
0
18
36
54
72
90
0
500
1000
1500
2000
2500
3000

Figure 11

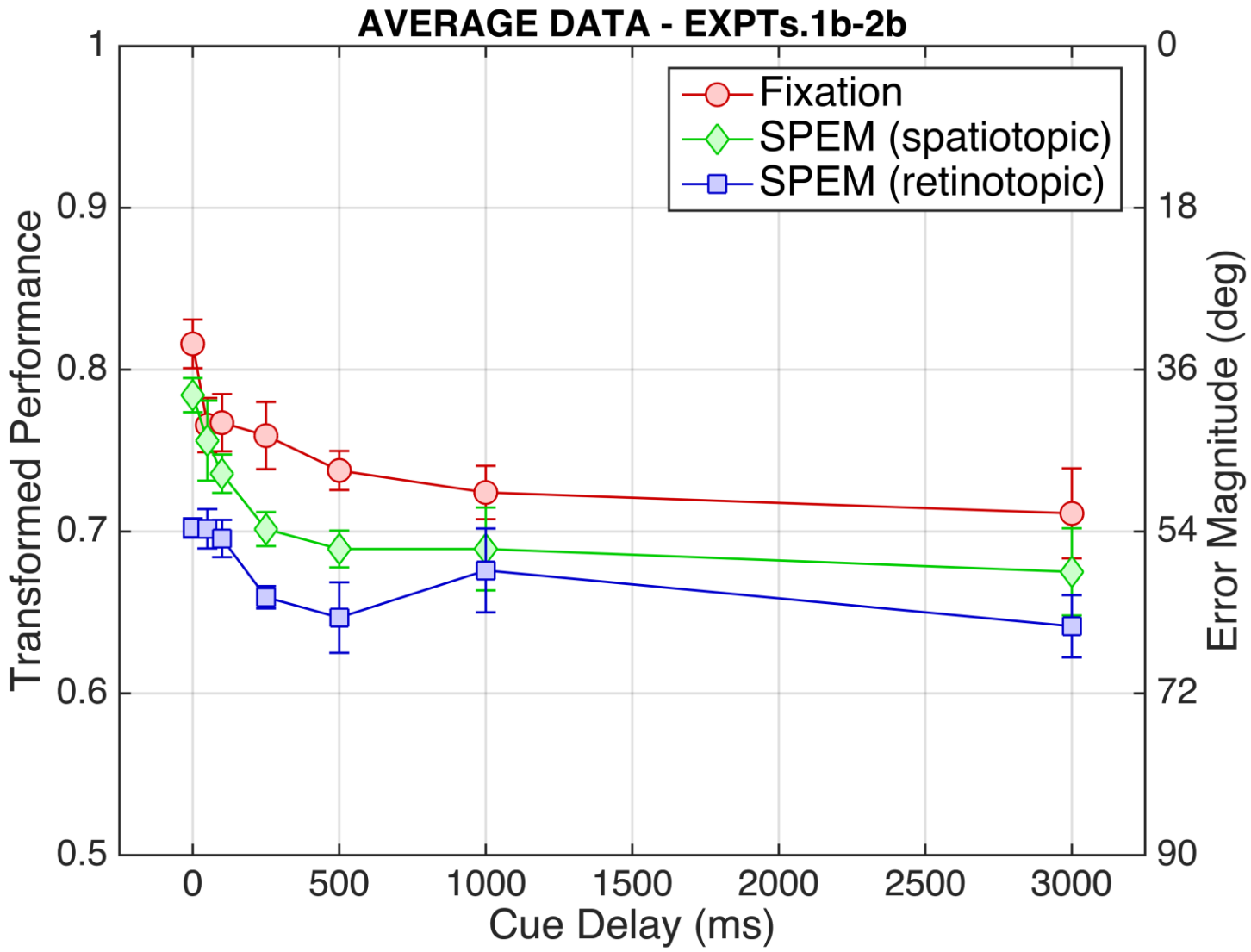
AVERAGE DATA - EXPTs.1b-2b
Fixation
SPEM (spatiotopic)
SPEM (retinotopic)
Transformed Performance
Error Magnitude (deg)
Cue Delay (ms)
1
0.9
0.8
0.7
0.6
0.5
0
18
36
54
72
90
0
500
1000
1500
2000
2500
3000

Figure 12

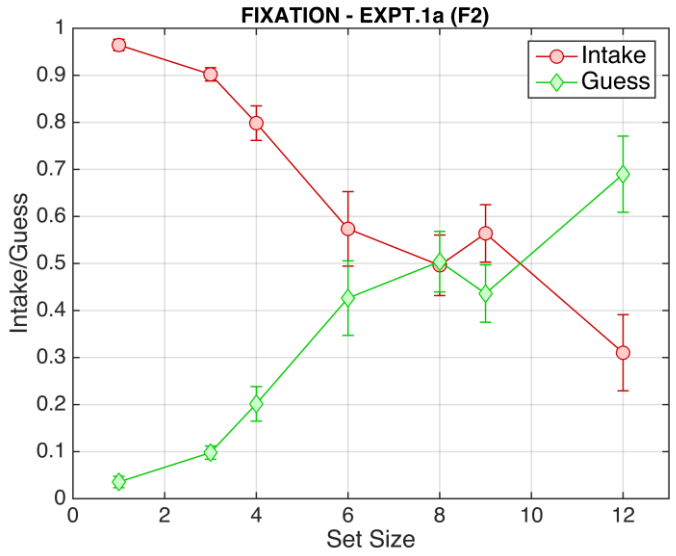
FIXATION - EXPT.1a (F2)
Intake
Guess
Intake/Guess
Set Size

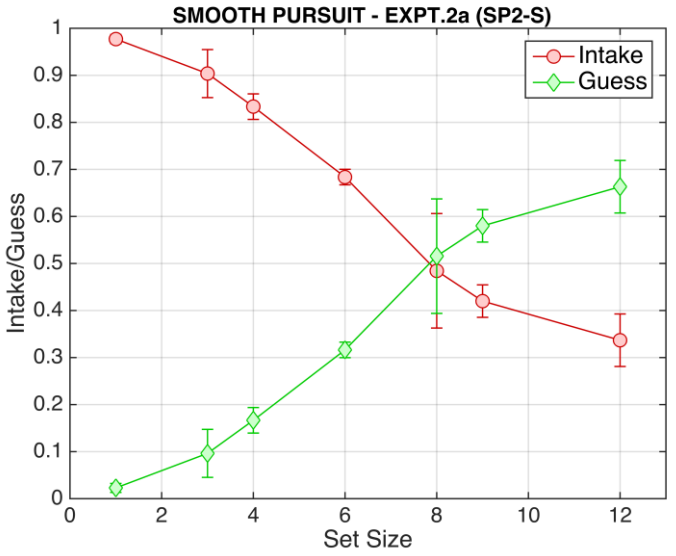
SMOOTH PURSUIT - EXPT.2a (SP2-S)
Intake
Guess
Intake/Guess
Set Size

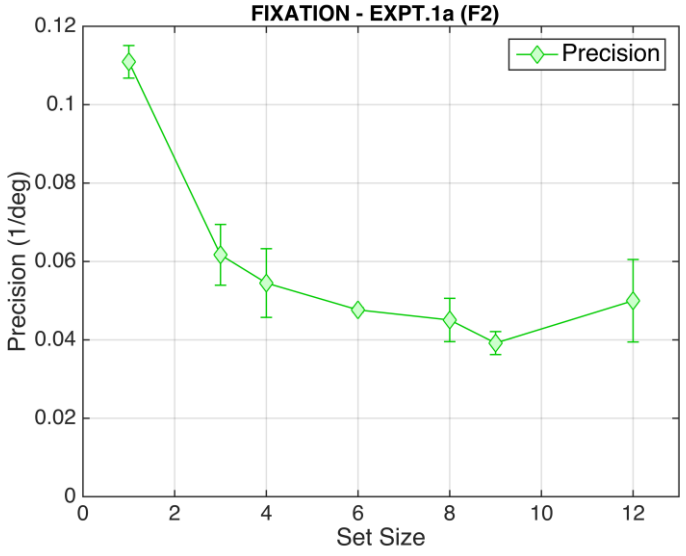
FIXATION - EXPT.1a (F2)
Precision
Precision (1/deg)
Set Size

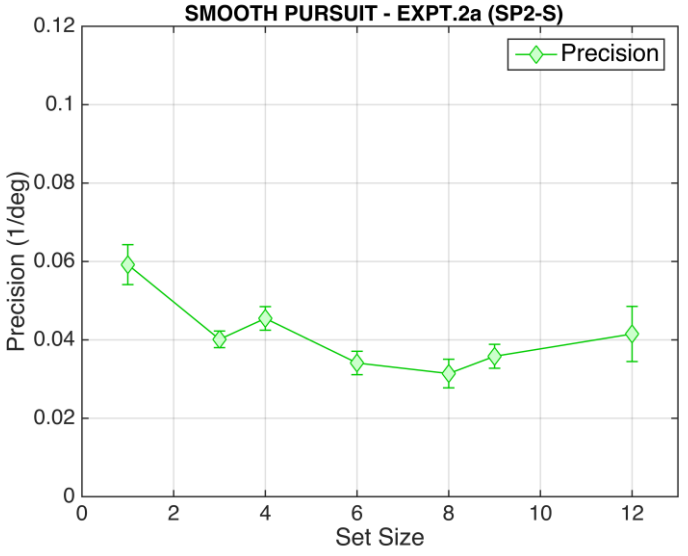
SMOOTH PURSUIT - EXPT.2a (SP2-S)
Precision
Precision (1/deg)
Set Size

Figure 13

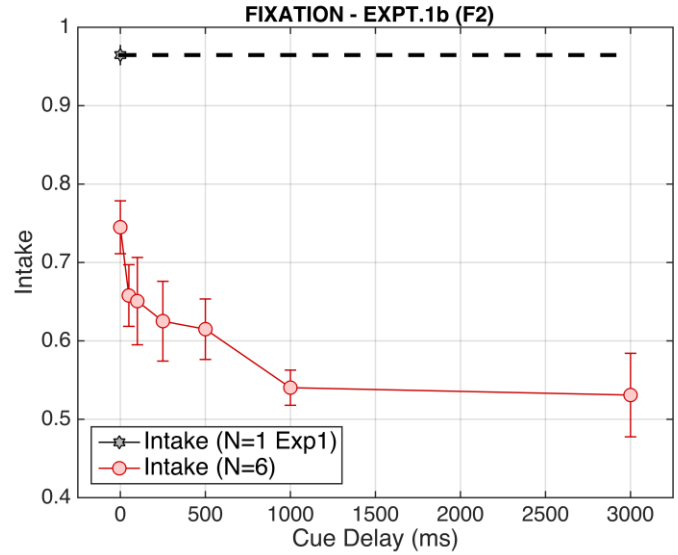
FIXATION - EXPT.1b (F2)
Intake
Cue Delay (ms)
Intake (N=1 Exp1)
Intake (N=6)

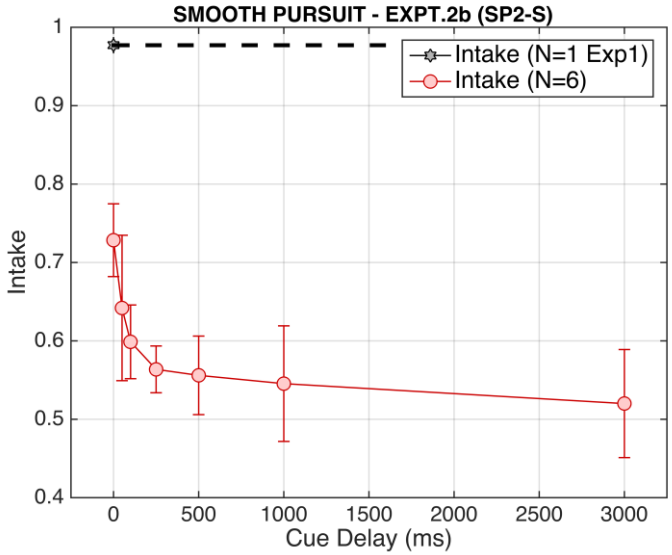
SMOOTH PURSUIT - EXPT.2b (SP2-S)
Intake
Cue Delay (ms)
Intake (N=1 Exp1)
Intake (N=6)

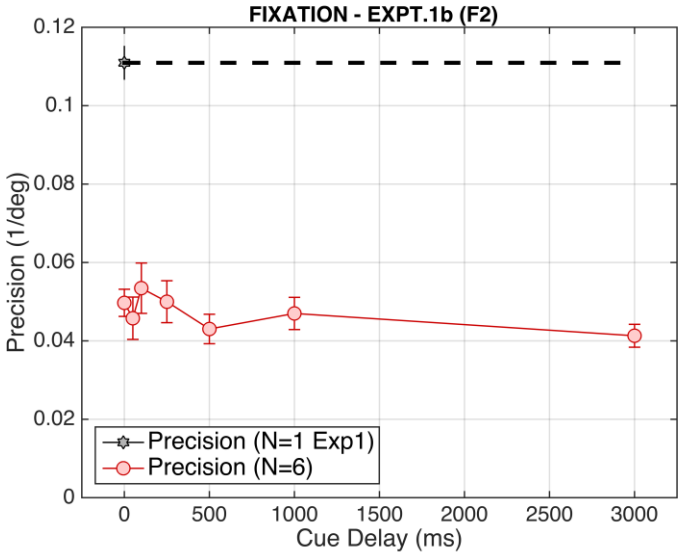
FIXATION - EXPT.1b (F2)
Precision (1/deg)
Cue Delay (ms)
Precision (N=1 Exp1)
Precision (N=6)

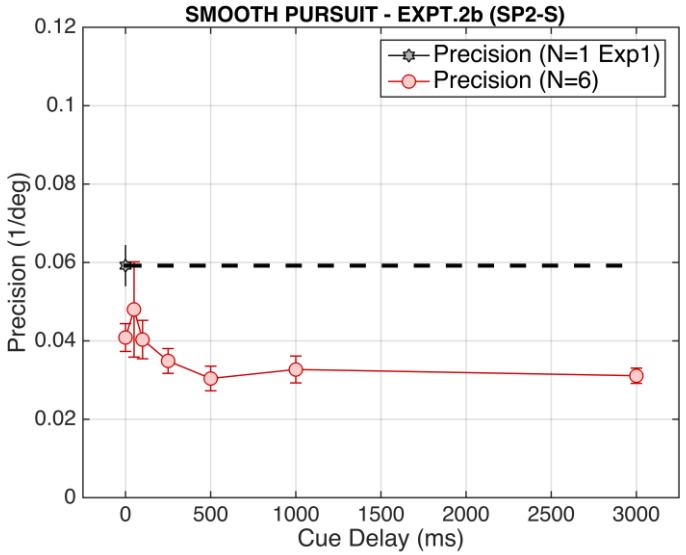
SMOOTH PURSUIT - EXPT.2b (SP2-S)
Precision (1/deg)
Cue Delay (ms)
Precision (N=1 Exp1)
Precision (N=6)

Figure 14

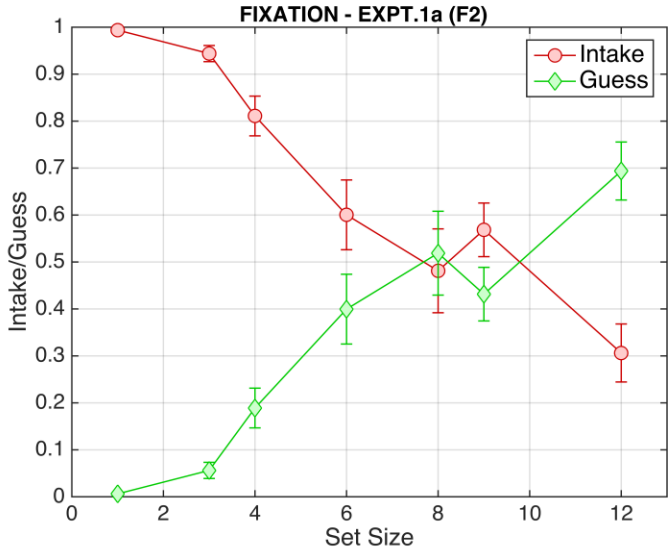
FIXATION - EXPT.1a (F2)
Intake
Guess
Intake/Guess
Set Size

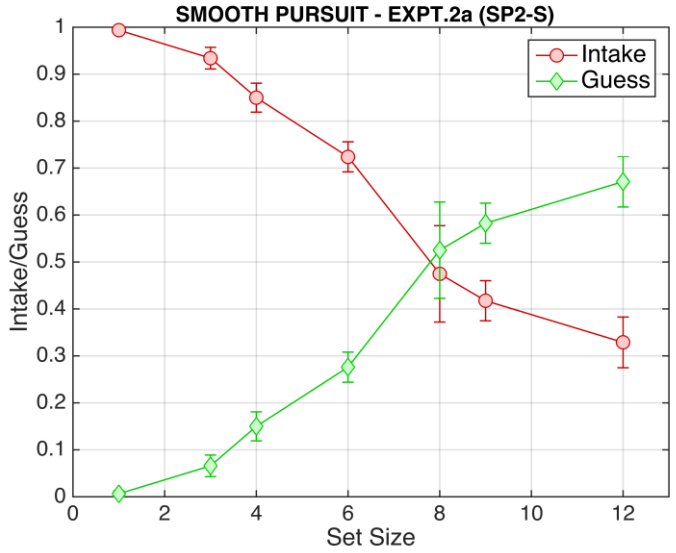
SMOOTH PURSUIT - EXPT.2a (SP2-S)
Intake
Guess
Intake/Guess
Set Size

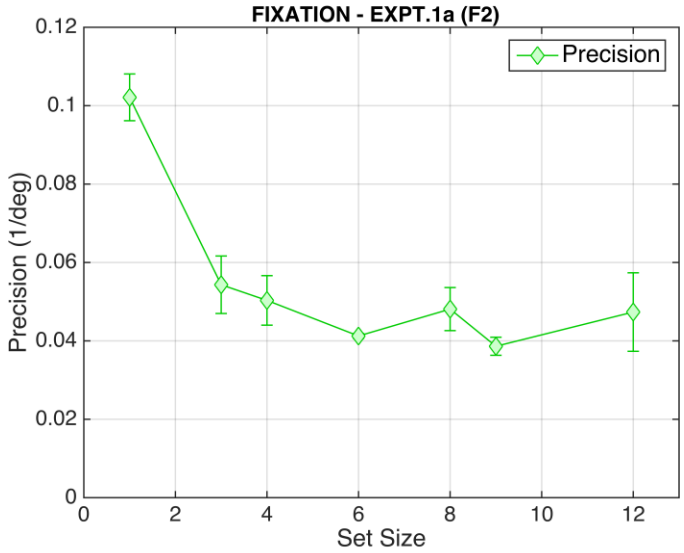
FIXATION - EXPT.1a (F2)
Precision
Precision (1/deg)
Set Size

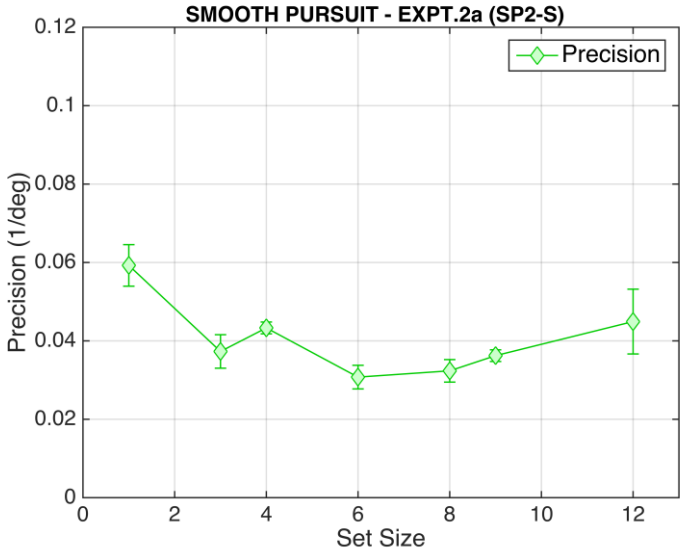
SMOOTH PURSUIT - EXPT.2a (SP2-S)
Precision
Precision (1/deg)
Set Size

Figure S1

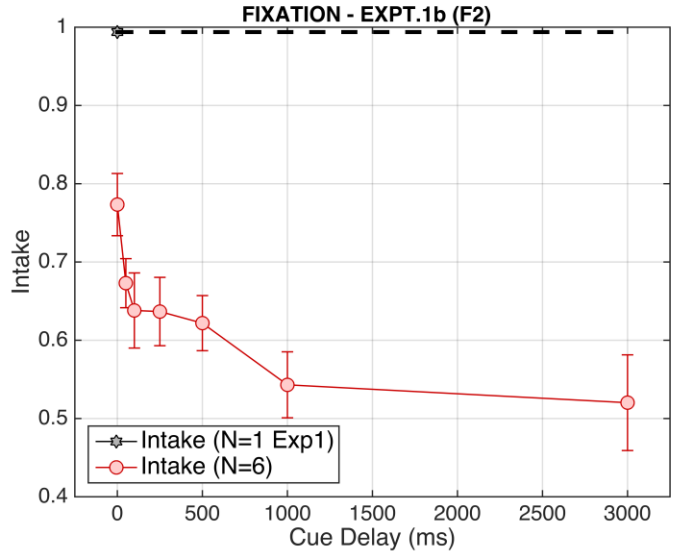
FIXATION - EXPT.1b (F2)
Intake
Cue Delay (ms)
Intake (N=1 Exp1)
Intake (N=6)

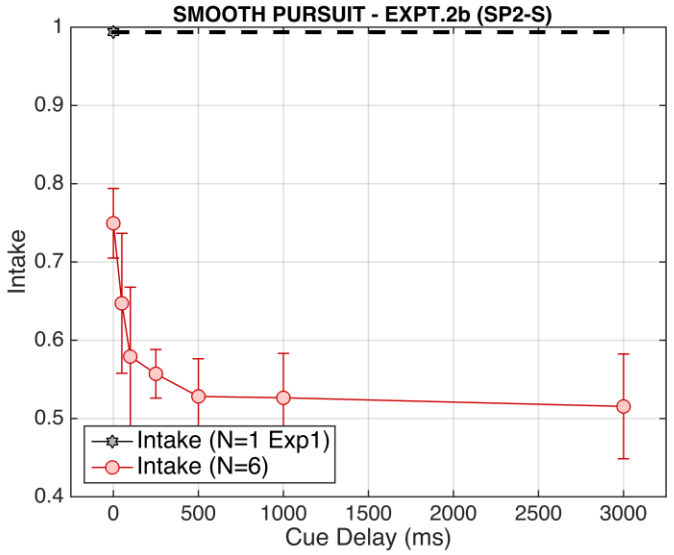
SMOOTH PURSUIT - EXPT.2b (SP2-S)
Intake
Cue Delay (ms)
Intake (N=1 Exp1)
Intake (N=6)

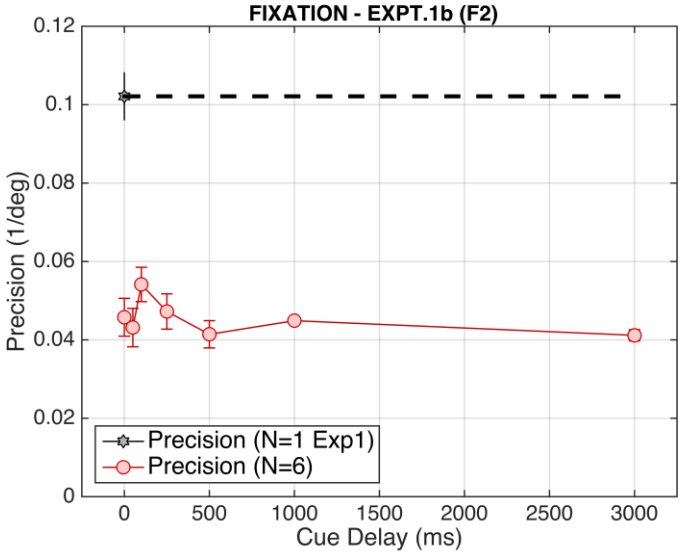
FIXATION - EXPT.1b (F2)
Precision (1/deg)
Cue Delay (ms)
Precision (N=1 Exp1)
Precision (N=6)

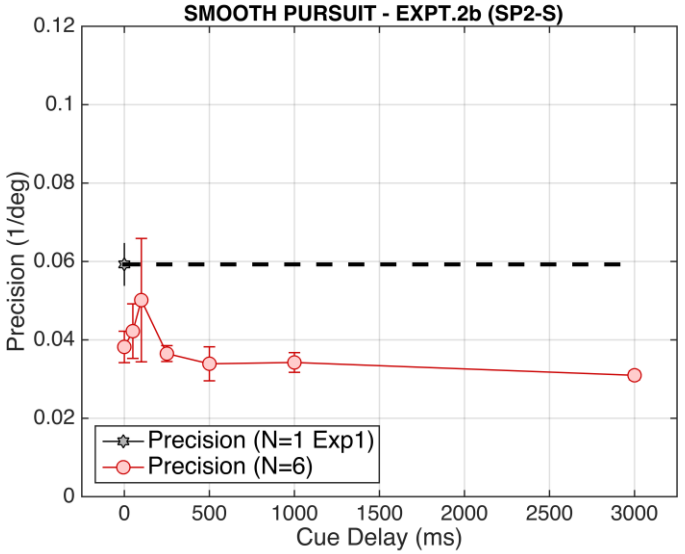
SMOOTH PURSUIT - EXPT.2b (SP2-S)
Precision (1/deg)
Cue Delay (ms)
Precision (N=1 Exp1)
Precision (N=6)

Figure S2

DECOMPOSITION BASED ON ACTUAL EYE VELOCITY

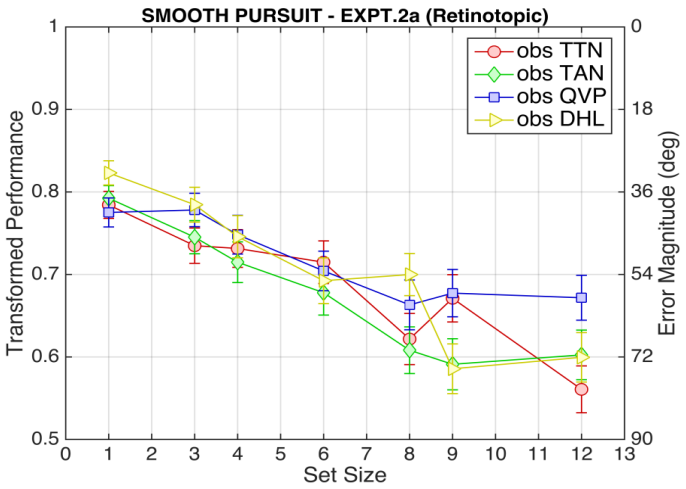

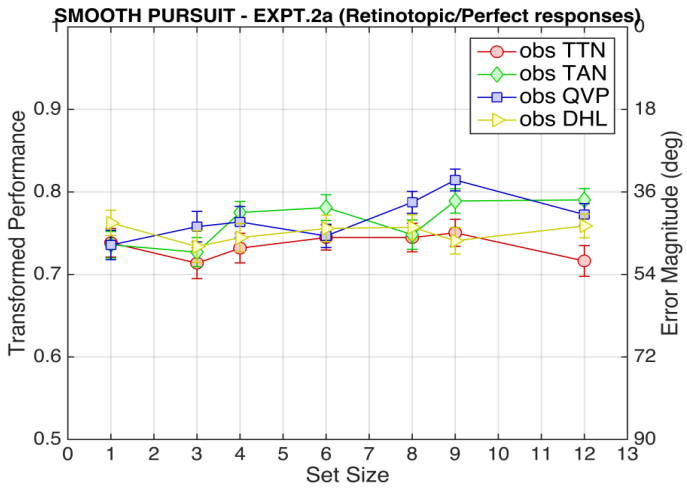

DECOMPOSITION BASED ON THEORETICAL EYE VELOCITY

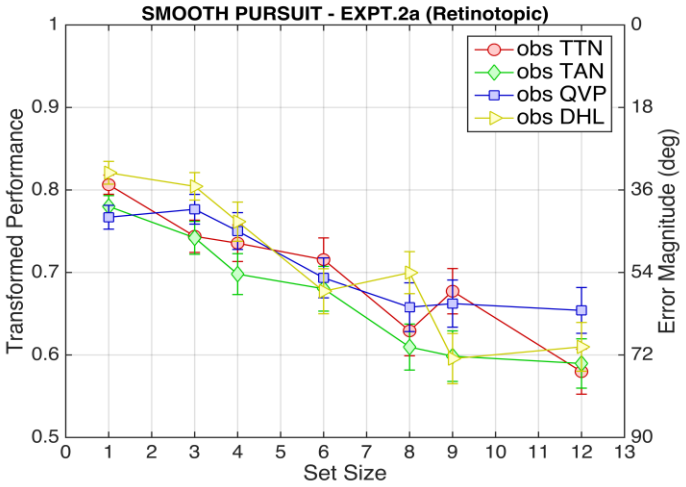

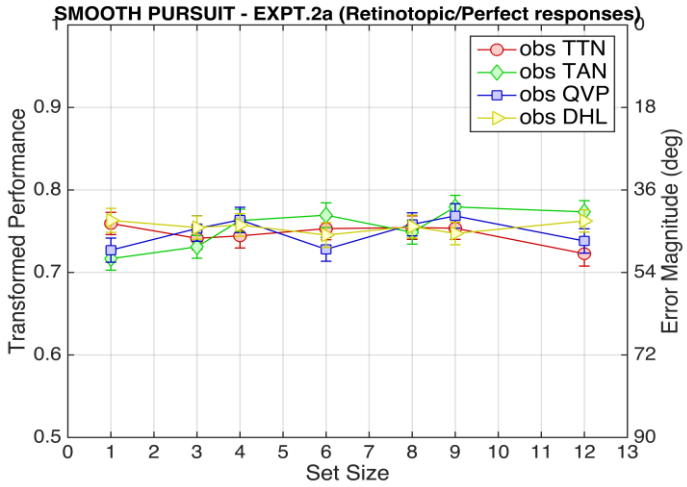

Figure S3

Condition	Fixation				SPEM											
Model	F1	F2	F3c	F3r	SP1_S	SP2_S	SP3c_S	SP3r_S	SP1_R	SP2_R	SP3c_R	SP3r_R	SP1_SR	SP2_SR	SP3c_SR	SP3r_SR
Experiment 1a-2a (Set-size = *N*)																
N = 3	0.9951	0.9963	0.9963	0.9965	0.9949	0.9963	0.9964	0.9966	0.9056	0.9040	0.9024	0.9024	0.9966	0.9966	0.9966	0.9966
N = 4	0.9915	0.9957	0.9956	0.9959	0.9947	0.9969	0.9969	0.9969	0.9091	0.9052	0.9016	0.9016	0.9943	0.9949	0.9949	0.9949
N = 6	0.9847	0.9962	0.9965	0.9963	0.9909	0.9952	0.9953	0.9950	0.9657	0.9716	0.9650	0.9652	0.9893	0.9912	0.9917	0.9914
N = 8	0.9846	0.9968	0.9972	0.9970	0.9917	0.9972	0.9972	0.9977	0.9892	0.9897	0.9898	0.9898	0.9925	0.9959	0.9963	0.9959
N = 9	0.9877	0.9963	0.9966	0.9966	0.9876	0.9963	0.9961	0.9961	0.9858	0.9872	0.9875	0.9886	0.9872	0.9919	0.9917	0.9914
N = 12	0.9887	0.9974	0.9974	0.9974	0.9887	0.9965	0.9968	0.9963	0.9875	0.9878	0.9873	0.9873	0.9909	0.9954	0.9955	0.9954
Experiment 1b-2b (Cue Delay = *D* ms)																
D = 0	0.9903	0.9961	0.9963	0.9976	0.9897	0.9959	0.9965	0.9962	0.9538	0.9532	0.9417	0.9417	0.9949	0.9959	0.9962	0.9961
D = 50	0.9894	0.9972	0.9972	0.9976	0.9875	0.9929	0.9953	0.9930	0.9645	0.9640	0.9633	0.9633	0.9847	0.9872	0.9889	0.9863
D = 100	0.9849	0.9962	0.9964	0.9962	0.9875	0.9963	0.9968	0.9971	0.9729	0.9754	0.9730	0.9730	0.9913	0.9939	0.9932	0.9934
D = 250	0.9854	0.9966	0.9969	0.9968	0.9888	0.9973	0.9978	0.9974	0.9768	0.9769	0.9769	0.9776	0.9927	0.9952	0.9956	0.9952
D = 500	0.9871	0.9967	0.9972	0.9969	0.9898	0.9964	0.9964	0.9972	0.9862	0.9861	0.9860	0.9904	0.9922	0.9950	0.9950	0.9950
D = 1000	0.9837	0.9958	0.9959	0.9958	0.9890	0.9958	0.9960	0.9958	0.9836	0.9834	0.9831	0.9838	0.9921	0.9936	0.9943	0.9928
D = 3000	0.9865	0.9975	0.9976	0.9978	0.9915	0.9970	0.9967	0.9967	0.9831	0.9829	0.9826	0.9822	0.9874	0.9893	0.9909	0.9892

Table 1

Set Size	1	3	4	6	8	9	12
Actual eye movement	0.7937	0.7607	0.7351	0.6973	0.6482	0.6313	0.6086
Theoretical eye movement	0.7936	0.7667	0.7363	0.6916	0.6491	0.6334	0.6083

Table S1